

Response to review comments on acp-2016-453 from reviewer 1

The original comments are provided in black, our response is given below each comment in red.

Thank you for your review. We have addressed the general and specific comments below and modified the manuscript accordingly.

In order to address your comments we have:

- 1) Conducted an additional year-long simulation at 60 km resolution using a different cumulus scheme**
- 2) Conducted an additional year-long simulation at 60 km resolution using a different set of meteorological lateral boundary conditions.**
- 3) Conducted an additional suite of evaluations including inclusion of BSS using MODIS climatology as the reference (we note here that of course as we specified in the manuscript 2008 was chosen as a climatologically representative year).**

The responses to the reviews do not address the points made by the reviewers adequately, in particular the differences in meteorological variables at 12 km and 60 km horizontal resolution and the precipitation bias at 60 km resolution need to be understood (see below). Publication can only be recommended after major revisions.

General comment:

For a meaningful comparison of AOD between the simulations at 12 km and 60 km horizontal resolution the differences in meteorological variables and their impact on AOD need to be understood. The annual mean precipitation in the studied region should be around 800 -1200 mm with a standard deviation of about 180 - 260 mm (Groisman and Easterling, 1994). The precipitation of the 60 km simulation in Fig. S3 is significantly below these values in many areas. The reason for the difference between the 12km and 60 km simulations could be the different performance of parameterization at different resolutions or internal variability. The discussion of the cumulus scheme by the authors is very welcome and should be added to the main text. It remains to be checked if the difference between the 12 km and 60 km simulations is also due to internal variability. A 60 km simulation is significantly cheaper than a 12 km simulation. 60 km simulations with varying initial conditions can be used to explore the internal variability and if possible reduce the differences in meteorological variables, in particular reduce the precipitation bias.

We explored model sensitivity to the cumulus parameterizations by applying the Grell-Freitas cumulus scheme (Grell and Freitas, 2014), which is the next generation of the Grell 3D scheme and has been tested with WRF-Chem, following recommendations of NCAR scientists for our particular case study (personal correspondence with [Saide P., Kumar R., Archer Nicholls S.], 2016). Analysis of precipitation seasonal fields (Figure 1 below) do not present significant differences in magnitude and patterns compared to the original simulations adopting the Grell 3D scheme. As a result, also the BSS of both precipitation and AOD at different wavelengths lead to the same original conclusions on the higher performance of WRF12-remap vs WRF60.

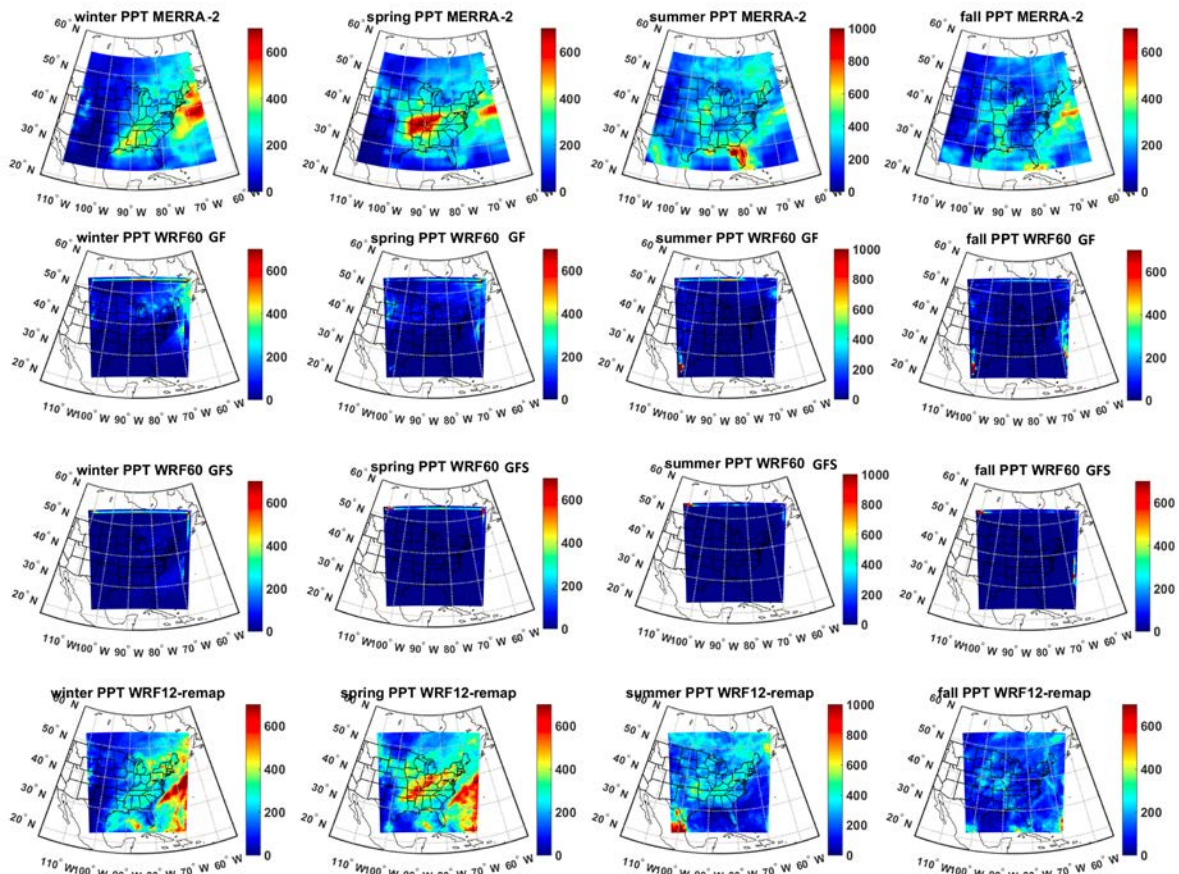


Figure 1. Seasonal total precipitation (mm) for MERRA-2 (first row), WRF60 with Grell-Freitas cumulus scheme (second row), WRF60 with meteorological boundary conditions from GFS (third row) and WRF12-remap (fourth row). The Grell 3D cumulus scheme is applied to both WRF60-GFS and WRF12-remap.

Modification to the text is as follows:

In the introduction (lines 126-146):

“Based on the performance evaluation of the WRF-Chem simulations that indicate substantial dry bias in the WRF60 simulations and large seasonality in the value-added by enhanced resolution, we conducted two further year-long simulations at 60 km. In the first we held all other simulation conditions constant but selected a different cumulus parameterization. In the second, we held all simulation conditions constant but employed a different set of lateral boundary conditions for the meteorology. In the context of the precipitation biases reported herein it is worthy of note that discrepancies in simulated precipitation regimes are key challenges in regional modelling (both physical and coupled with chemistry). Although the Grell 3D scheme has been successfully applied in a number of prior analysis wherein the model was applied at resolutions in the range of 1-36 km (e.g. (Grell and Dévényi, 2002;Lowrey and Yang, 2008;Nasrollahi et al., 2012;Sun et al., 2014;Zhang et al., 2016)), the North American Regional Climate Change Assessment Program (NARCCAP) simulations with WRF at 50-km were also dry biased in the study domain (Mearns et al., 2012). Although there have been a number of studies that have sought to evaluate different cumulus schemes over different regions at different resolutions, no definitive recommendation has been made regarding the dependence of model’s skill on resolution and cumulus parameterization (Arakawa, 2004;Jankov et al., 2005;Nasrollahi et

al., 2012;Li et al., 2014). Thus, further research is needed to identify the optimal cumulus scheme for use over North America at coarser resolution. Thus, we performed a sensitivity analysis on the cumulus scheme at 60 km by applying the Grell-Freitas parameterization (Grell and Freitas, 2014), which is the next generation of the Grell 3D scheme.”

In the methods (lines 202-210):

“As described in detail below, in the WRF60 simulations configured as described in Table 1, simulated precipitation during the summer months exhibits substantial dry bias, and the analysis of value added by enhanced simulation resolution exhibited strong seasonality. We performed a sensitivity analysis to the cumulus scheme, by conducting an additional year-long simulation at 60 km using the Grell-Freitas parameterization (Grell and Freitas, 2014), which is an evolution of Grell 3D that is scale-aware and treats some aspects of aerosol-cloud interactions. We also tested the sensitivity of the simulation results to the meteorological boundary conditions, by repeating the WRF60 simulations using output from the Global Forecast System (GFS) at 0.5° resolution every 6 hours to provide the lateral boundary conditions.”

In the results (lines 509-519):

“Use of the Grell-Freitas parameterization in the WRF60 simulations did not lead to substantially different magnitude and/or spatial patterns of precipitation compared to WRF60 applied with the Grell 3D scheme, and no improvement in agreement with output from MERRA2. The findings of a negative bias in WRF60 simulations without a corresponding overestimation of AOD may appear counter-intuitive since aerosol concentrations (and thus AOD) are dependent on aerosol residence times and analyses of sixteen global models from the AeroCom project indicate wet scavenging is the dominant removal process for most aerosol species in the study area (Hand et al., 2012;Textor et al., 2006). However, the negative precipitation bias in WRF60 simulations appears to be linked to poor representation of surface moisture availability, boundary layer humidity (Fig. 6), and ultimately aerosol water content (and hence AOD).”

In order to test the internal variability, we drove WRF60 with boundary meteorological conditions from the Global Forecast System (GFS) at 0.5 degree resolution every 6 hours and kept the Grell 3D cumulus scheme. Results from this run also show a systematic under-prediction of precipitation over the domain (Figure 1). Some variability in skill metrics are found for AOD (Figure 2 below), although similar conclusions can be drawn regarding the higher performance of WRF12-remap vs WRF60.

Based on these results, it appears that the skill of WRF-Chem with the physics/dynamics schemes adopted in this work is highly sensitive on the spatial resolution and that the sensitivity of the results to the LBC is relatively small.

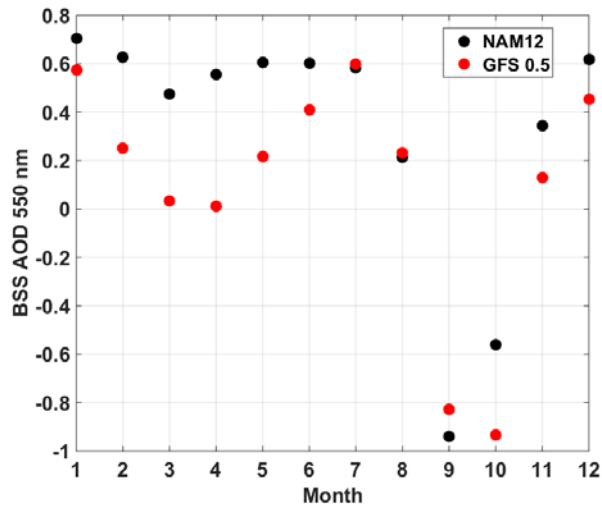


Figure 2. BSS for AOD at 550 nm from WRF-Chem simulations at 60km driven by boundary meteorological conditions from NAM12 (black dots) and GFS (red dots). The BSS is computed according to Equation 5 in the manuscript.

Modification to the text is as follows:

In the introduction (lines 126-131):

“Based on the performance evaluation of the WRF-Chem simulations that indicate substantial dry bias in the WRF60 simulations and large seasonality in the value-added by enhanced resolution, we conducted two further year-long simulations at 60 km. In the first we held all other simulation conditions constant but selected a different cumulus parameterization. In the second, we held all simulation conditions constant but employed a different set of lateral boundary conditions for the meteorology.”

In the methods (lines 207-210):

“We also tested the sensitivity of the simulation results to the meteorological boundary conditions, by repeating the WRF60 simulations using output from the Global Forecast System (GFS) at 0.5° resolution every 6 hours to provide the lateral boundary conditions.”

In the results (lines 422-424):

“Interestingly, BSS for most months (excluding September) are higher for the WRF60 simulations conducted using lateral boundary conditions from NAM12 than GFS.”

For both issues please also refer to the modified Figure 5.

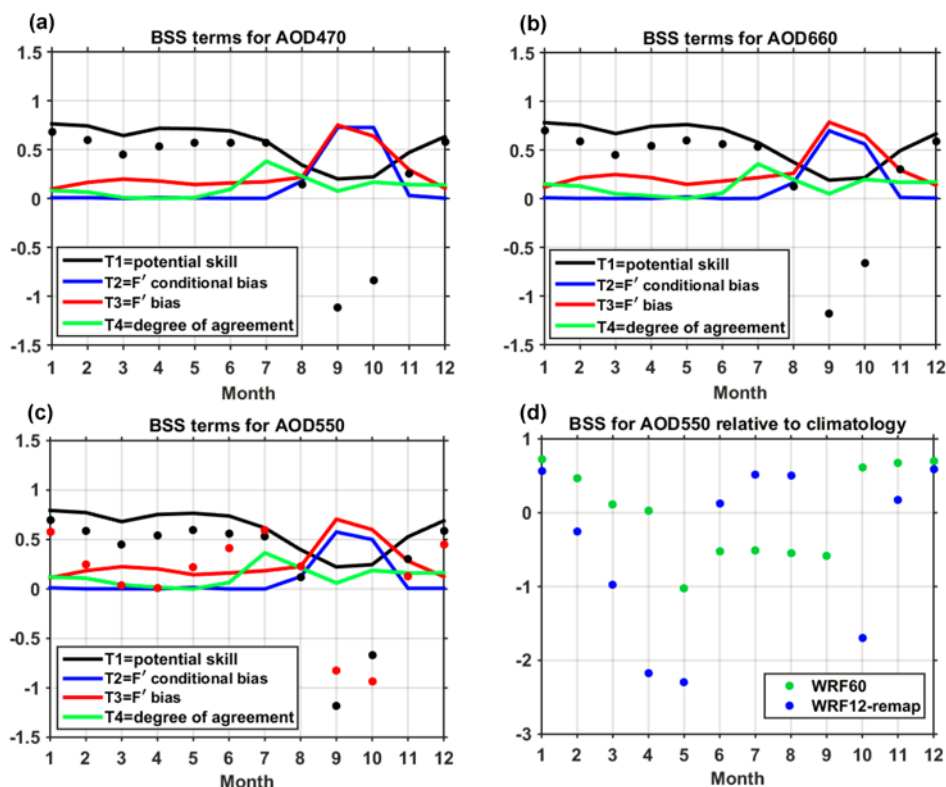


Figure 1. (a-c) Brier Skill Scores (BSS, black dots) for monthly mean AOD by calendar month (1=January) for AOD at 470, 550 and 660 nm. In this analysis of model skill WRF12 output is mapped to the WRF60 grid (WRF12-remap) and BSS are computed using MODIS as the target, WRF60 (driven by NAM12 meteorological boundary conditions) as the reference forecast and WRF12-remap as the forecast. Also shown by the color lines are the contributions of different terms to BSS. In panel c the red dots indicate BSS when the reference forecast is WRF60 driven by GFS meteorological boundary conditions. (d) BSS of monthly mean AOD from WRF60 (green dots) and WRF12-remap (blue dots) relative to MODIS monthly mean climatology during 2000-2014 (reference forecast). Monthly mean AOD from MODIS are used as the target. BSS for WRF12-remap in September is -6.1.

Specific comments:

P6, L 152: Effects of the boundary conditions are clearly visible in some of the Figures e.g. Fig. 4, Fig. 6, Figs. S1-S3. It should be mentioned in the text that removing the cells at the boundary does not significantly affect the BSS results or the boundary cells should be excluded from the analysis. Otherwise a reader may be confused whether or not the cells at the boundary are included in the analysis and whether or not they affect the results.

We agree. We have now clarified that removing the boundary cells does not affect the BSS results. Noted in the results (from line 412):

“Although the effects of the boundary conditions appear in some variables (e.g. in Fig. 4 and Figs. S1-S3), the BSS results do not significantly change even when those cells are removed from the analysis.”

P10, L273-L298: Using the BSS and its decomposition in Murphy and Epstein is useful to investigate which one of two simulations has the higher skill. But it would be interesting and within the scope of the paper to know also the skill of each simulation individually. Therefore it would be useful to compute in addition a BSS for each simulation (WRF60 and WRF12-remap) by using climatological values as the reference.

Done. We computed BSS for WRF60 and WRF12-remap relative to MODIS climatology over the years 2000-2014. Modification of the text (lines 415-422):

“When the BSS is used to assess the skill of each model relative to MODIS AOD climatological mean over the years 2000-2014, WRF12-remap is found to add value relative to the climatology (i.e. BSS >0) during summer months and Nov-Jan whereas BSS for WRF60 is positive from late Fall to early Spring (Fig. 5d). The fact that WRF-Chem does not always outperform the climatology is expected since the model is based on time invariant emissions and skills are assessed relative to a year selected to be representative of the AOD climatology. Mean seasonal AOD from MODIS retrievals over the study region during 2008 lie within ± 0.2 standard deviations of the climatology (Crippa et al., 2016).”

P17, L477-L485: Because wet scavenging by precipitation is removing most of the aerosol globally (Textor et al., 2006) a short discussion how wet scavenging by precipitation affects the comparison of the two resolutions should be added.

We have now added the following discussion on how wet scavenging impacts aerosol properties. Added text reads (lines 512-519):

“The findings of a negative bias in WRF60 simulations without a corresponding overestimation of AOD may appear counter-intuitive since aerosol concentrations (and thus AOD) are dependent on aerosol residence times and analyses of sixteen global models from the AeroCom project indicate wet scavenging is the dominant removal process for most aerosol species in the study area (Hand et al., 2012;Textor et al., 2006). However, the negative precipitation bias in WRF60 simulations appears to be linked to poor representation of surface moisture availability, boundary layer humidity (Fig. 6), and ultimately aerosol water content (and hence AOD).”

Technical corrections:

P6, L134: The Angstrom exponent alpha is the exponent for (λ_1/λ_2) , i.e. $(\lambda_1/\lambda_2)^{-\alpha}$.

Thanks, done.

P6, L138: The natural logarithm is missing in the denominator.

Agree, added now. Thanks.

P6, L141: Only 2π is below the square root, not σ_i . Sigma is the standard deviation, not the geometric standard deviation. r is not defined.

Fixed and added definition of r.

P6, L145: The variables in this equation depend on z. z is not defined.

Fixed, thanks.

P7, L167: There are words missing before representative.

Added “it is”.

Reference:

Textor, C., Schulz, M., Guibert, S., Kinne, S., Balkanski, Y., Bauer, S., Berntsen, T., Berglen, T., Boucher, O., Chin, M., Dentener, F., Diehl, T., Easter, R., Feichter, H., Fillmore, D., Ghan, S., Ginoux, P., Gong, S., Grini, A., Hendricks, J., Horowitz, L., Huang, P., Isaksen, I., Iversen, I., Kloster, S., Koch, D., Kirkevåg, A., Kristjansson, J. E., Krol, M., Lauer, A., Lamarque, J. F., Liu, X., Montanaro, V., Myhre, G., Penner, J., Pitari, G., Reddy, S., Seland, Ø., Stier, P., Takemura, T., and Tie, X.: Analysis and quantification of the diversities of aerosol life cycles within AeroCom, *Atmos. Chem. Phys.*, 6, 1777-1813, doi:10.5194/acp-6-1777-2006, 2006.

References

Arakawa, A.: The Cumulus Parameterization Problem: Past, Present, and Future, *Journal of Climate*, 17, 2493-2525, doi:10.1175/1520-0442(2004)017<2493:RATCPP>2.0.CO;2, 2004.

Grell, G. A., and Dévényi, D.: A generalized approach to parameterizing convection combining ensemble and data assimilation techniques, *Geophysical Research Letters*, 29, 38-31-38-34, 10.1029/2002GL015311, 2002.

Grell, G. A., and Freitas, S. R.: A scale and aerosol aware stochastic convective parameterization for weather and air quality modeling, *Atmospheric Chemistry and Physics*, 14, 5233-5250, 10.5194/acp-14-5233-2014, 2014.

Hand, J. L., Schichtel, B. A., Pitchford, M., Malm, W. C., and Frank, N. H.: Seasonal composition of remote and urban fine particulate matter in the United States, *J. Geophys. Res.-Atmos.*, 117, 10.1029/2011jd017122, 2012.

Jankov, I., A. Gallus, J. W., Segal, M., Shaw, B., and E. Koch, S.: The Impact of Different WRF Model Physical Parameterizations and Their Interactions on Warm Season MCS Rainfall, *Weather and Forecasting*, 20, 1048-1060, doi:10.1175/WAF888.1, 2005.

Li, L. F., Li, W. H., and Jin, J. M.: Improvements in WRF simulation skills of southeastern United States summer rainfall: physical parameterization and horizontal resolution, *Clim Dyn*, 43, 2077-2091, 10.1007/s00382-013-2031-2, 2014.

Lowrey, M. R. K., and Yang, Z. L.: Assessing the Capability of a Regional-Scale Weather Model to Simulate Extreme Precipitation Patterns and Flooding in Central Texas, *Weather and Forecasting*, 23, 1102-1126, 10.1175/2008waf2006082.1, 2008.

Mearns, L. O., Arritt, R., Biner, S., Bukovsky, M. S., McGinnis, S., Sain, S., Caya, D., Jr., J. C., Flory, D., Gutowski, W., Takle, E. S., Jones, R., Leung, R., Moufouma-Okia, W., McDaniel, L., Nunes, A. M. B., Qian, Y., Roads, J., Sloan, L., and Snyder, M.: The North American Regional Climate Change Assessment Program: Overview of Phase I Results, *Bulletin of the American Meteorological Society*, 93, 1337-1362, doi:10.1175/BAMS-D-11-00223.1, 2012.

- Nasrollahi, N., AghaKouchak, A., Li, J. L., Gao, X. G., Hsu, K. L., and Sorooshian, S.: Assessing the Impacts of Different WRF Precipitation Physics in Hurricane Simulations, *Weather and Forecasting*, 27, 1003-1016, 10.1175/waf-d-10-05000.1, 2012.
- Sullivan, R. C., Levy, R. C., and Pryor, S. C.: Spatiotemporal coherence of mean and extreme aerosol particle events over eastern North America as observed from satellite, *Atmos. Environ.*, 112, 126-135, <http://dx.doi.org/10.1016/j.atmosenv.2015.04.026>, 2015.
- Sun, Y., Yi, L., Zhong, Z., and Ha, Y.: Performance of a New Convective Parameterization Scheme on Model Convergence in Simulations of a Tropical Cyclone at Grey-Zone Resolutions, *Journal of the Atmospheric Sciences*, 71, 2078-2088, doi:10.1175/JAS-D-13-0285.1, 2014.
- Textor, C., Schulz, M., Guibert, S., Kinne, S., Balkanski, Y., Bauer, S., Berntsen, T., Berglen, T., Boucher, O., Chin, M., Dentener, F., Diehl, T., Easter, R., Feichter, H., Fillmore, D., Ghan, S., Ginoux, P., Gong, S., Kristjansson, J. E., Krol, M., Lauer, A., Lamarque, J. F., Liu, X., Montanaro, V., Myhre, G., Penner, J., Pitari, G., Reddy, S., Seland, O., Stier, P., Takemura, T., and Tie, X.: Analysis and quantification of the diversities of aerosol life cycles within AeroCom, *Atmospheric Chemistry and Physics*, 6, 1777-1813, 2006.
- Wang, J. L., and Kotamarthi, V. R.: Downscaling with a nested regional climate model in near-surface fields over the contiguous United States, *J. Geophys. Res.-Atmos.*, 119, 8778-8797, 10.1002/2014jd021696, 2014.
- Zhang, Y., He, J., Zhu, S., and Gantt, B.: Sensitivity of simulated chemical concentrations and aerosol-meteorology interactions to aerosol treatments and biogenic organic emissions in WRF/Chem, *Journal of Geophysical Research: Atmospheres*, 121, 6014-6048, 10.1002/2016JD024882, 2016.

1 **Value-added by high-resolution regional simulations of**
2 **climate-relevant aerosol properties**

3
4 P. Crippa¹, R. C. Sullivan², A. Thota³, S. C. Pryor^{2,3}

5
6
7 ¹COMET, School of Civil Engineering and Geosciences, Cassie Building, Newcastle
8 University, Newcastle upon Tyne, NE1 7RU, UK

9 ²Department of Earth and Atmospheric Sciences, Bradfield Hall, 306 Tower Road, Cornell
10 University, Ithaca, NY 14853, USA

11 ³Pervasive Technology Institute, Indiana University, Bloomington, IN 47405, USA

12
13 *Correspondence to:* P. Crippa (paola.crippa@ncl.ac.uk), School of Civil Engineering and
14 Geosciences, Cassie Building, Room G15, Telephone: +44 (0)191 208 5041, Newcastle
15 University, Newcastle upon Tyne, NE1 7RU, UK

16 **Abstract**

17 Despite recent advances in global Earth System Models (ESMs), the current global mean
18 aerosol direct and indirect radiative effects remain uncertain, as does their future role in
19 climate forcing and regional manifestations. Reasons for this uncertainty include the high
20 spatio-temporal variability of aerosol populations. Thus, limited area (regional) models
21 applied at higher resolution over specific regions of interest are generally expected to ‘add
22 value’, i.e. improve the fidelity of the physical-dynamical-chemical processes that induce
23 extreme events and dictate climate forcing, via more realistic representation of spatio-
24 temporal variability. However, added value is not inevitable, and there remains a need to
25 optimize use of numerical resources, and to quantify the impact on simulation fidelity that
26 derives from increased resolution. Here we quantify the value added by enhanced spatial
27 resolution in simulations of the drivers of aerosol direct radiative forcing by applying the
28 Weather Research and Forecasting model with coupled Chemistry (WRF-Chem) over eastern
29 North America at different resolutions. Using Brier Skill Scores and other statistical metrics it
30 is shown that enhanced resolution (from 60 to 12 km) improves model performance for all of
31 the meteorological parameters and gas phase concentrations considered, in addition to both
32 mean and extreme Aerosol Optical Depth (AOD) in three wavelengths in the visible relative
33 to satellite observations, principally via increase of potential skill. Some of the enhanced
34 model performance for AOD appears to be attributable to improved simulation of specific
35 humidity and the resulting impact on aerosol hygroscopic growth/hysteresis.

36

37 **Keywords:** added value, high-resolution WRF-Chem simulations, aerosol optical properties,
38 extreme AOD

39 **1 Motivation and Objectives**

40 Aerosols alter Earth’s radiation balance primarily by scattering or absorbing incoming solar
41 radiation (direct effect, dominated by accumulation mode (diameters \sim wavelength (λ), where
42 total extinction is often quantified using AOD), or regulating cloud formation/properties by
43 acting as cloud condensation nuclei (CCN) (indirect effect, dominated by diameters \geq 100
44 nm, magnitude = $f(\text{composition})$). Most aerosols (excluding black carbon) have a larger
45 scattering cross-section than absorption cross-section, and act as CCN thus enhancing cloud
46 albedo and lifetimes. Hence increased aerosol concentrations are generally (but not
47 uniformly) associated with surface cooling (offsetting a fraction of greenhouse gas warming)
48 (Boucher, 2013;Myhre et al., 2013b) to a degree that is principally dictated by the aerosol
49 concentration, size and composition, in addition to the underlying surface and height of the
50 aerosol layer (McComiskey et al., 2008). Despite major advances in measurement and
51 modeling, both the current global mean aerosol direct effect (possible range: -0.77 to +0.23
52 W m^{-2}) and the indirect effect (possible range: -1.33 to -0.06 W m^{-2}) remain uncertain
53 (Stocker, 2013), as does their future role in climate forcing (Rockel et al., 2008) and regional
54 manifestations (Myhre et al., 2013a). Specific to our current study region (eastern N.
55 America), one analysis using the NASA GISS global model found that the “regional radiative
56 forcing from US anthropogenic aerosols elicits a strong regional climate response, cooling
57 the central and eastern US by 0.5–1.0 $^{\circ}\text{C}$ on average during 1970–1990, with the strongest
58 effects on maximum daytime temperatures in summer and autumn. Aerosol cooling reflects
59 comparable contributions from direct and indirect radiative effects” (Leibensperger et al.,
60 2012). A recent comparison of multiple global models conducted under the AEROCOM-
61 project indicated this is also a region that exhibits very large model-to-model variability in
62 simulated AOD ($\langle\text{AOD}\rangle \sim 0.5$, $\sigma(\text{AOD}) \sim 1$) (Myhre et al., 2013a).

63 Major reasons why aerosol radiative forcing on both the global and regional scales remains
64 uncertain include short atmospheric residence times and high spatio-temporal variability of
65 aerosol populations, and the complexity of the processes that dictate aerosol concentrations,
66 composition and size distributions (Seinfeld and Pandis, 2016). Although aerosol processes
67 and properties are increasingly being treated in the global Earth System Models (ESMs)
68 (Long et al., 2015;Tilmes et al., 2015) being applied in Coupled Model Intercomparison
69 Project Phase 6 (CMIP-6) (Meehl et al., 2014), the scales on which such models are applied
70 remain much coarser than those on which aerosol population properties are known to vary
71 (Anderson et al., 2003). Therefore, limited area atmospheric models (regional models)

72 applied at higher resolution over specific regions of interest are expected to ‘add value’ (i.e.
73 improve the fidelity) of the physical-dynamical-chemical processes that induce extreme
74 events and dictate climate forcing. There is empirical evidence to suggest [a](#) strong resolution
75 dependence in simulated aerosol particle properties. For example, WRF-Chem simulations
76 with spatial resolution enhanced from 75 km to 3 km exhibited higher correlations and lower
77 bias relative to observations of aerosol optical properties over Mexico likely due to more
78 accurate description of emissions, meteorology and of the physicochemical processes that
79 convert trace gases to particles (Gustafson et al., 2011; Qian et al., 2010). This improvement
80 in the simulation of aerosol optical properties implies a reduction of the uncertainty in
81 associated aerosol radiative forcing (Gustafson et al., 2011). Further, WRF-Chem run over
82 the United Kingdom and Northern France at multiple resolutions in the range of 40-160 km,
83 underestimated AOD by 10-16% and overestimated CCN by 18-36% relative to a high
84 resolution run at 10 km, partly as a result of scale dependence of the gas-phase chemistry and
85 differences in the aerosol uptake of water (Weigum et al., 2016).

86 However, debate remains regarding how to objectively evaluate model performance, quantify
87 the value added by enhanced resolution (Di Luca et al., 2015; Rockel et al., 2008) and on
88 possible limits to the improvement of climate representation in light of errors in the driving
89 “imperfect lateral boundary conditions” (Diaconescu and Laprise, 2013). Nevertheless,
90 although “it is unrealistic to expect a vast amount of added values since models already
91 performs rather decently” (Di Luca et al., 2015) and global ESMs are now run at much higher
92 resolution than in the past, it is generally assumed that high resolution regional models will
93 add value via more realistic representation of spatio-temporal variability than global coarser-
94 resolution simulations. Further, “the main added value of a regional climate model is
95 provided by its small scales and its skill to simulate extreme events, particularly for
96 precipitation” (Diaconescu and Laprise, 2013).

97 Here we quantify the value added by enhanced resolution in the description of the drivers of
98 aerosol direct radiative forcing using year-long simulations from WRF-Chem over eastern
99 North America. The primary performance evaluation focuses on AOD at different
100 wavelengths ($\lambda = 470, 550$ and 660 nm, where the AOD at different λ is used as a proxy of
101 the aerosol size distribution (Tomasi et al., 1983), see details in Sect. 2.1) and is measured
102 relative to observations from satellite-borne instrumentation. Thus the term “value added” is
103 used here to refer to an improvement of model performance in simulation of wavelength
104 specific AOD as measured by the MODerate resolution Imaging Spectroradiometer (MODIS)

105 instrument aboard the polar-orbiting Terra satellite. We begin by quantifying the performance
106 of WRF-Chem when applied over eastern North America at a resolution of 60 km (WRF60)
107 (~ finest resolution likely to be employed in CMIP-6 global simulations) and then compare
108 the results to those from simulations conducted at 12 km (WRF12) (simulation details are
109 given in Table 1). Quantification of model skill is undertaken by mapping the WRF12 output
110 to the WRF60 grid (WRF12-remap) and computing Brier Skill Scores (BSS) using MODIS
111 as the target, WRF60 as the reference forecast and WRF12-remap as the forecast to be
112 evaluated. [We also evaluate the performance of the WRF-Chem simulations of 2008 relative](#)
113 [to climatology as represented by MODIS observations for 2000-2014.](#) We ~~also~~
114 ~~evaluate~~[additionally assess](#) the impact of simulation resolution on extreme AOD values that
115 are associated with enhanced impacts on climate and human health. This analysis uses both
116 *Accuracy* and *Hit Rate* as the performance metrics and focuses on the co-occurrence of
117 extreme values in space from the model output and MODIS.

118 Our ~~final~~ analysis ~~focuses on~~ [also incorporates](#) evaluation of the value-added by enhanced
119 resolution in terms of key meteorological and gas-phase drivers of aerosol concentrations and
120 composition and is conducted relative to the MERRA-2 reanalysis product for the physical
121 variables and columnar gas concentrations from satellite observations (see details of the
122 precise data sets used given below). The meteorological parameters considered are air
123 temperature at 2 m (T_{2m}), total monthly precipitation (*PPT*), planetary boundary-layer height
124 (*PBLH*) and specific humidity in the boundary layer (Q_{PBL}). The gas phase concentrations
125 considered are: sulfur dioxide (SO₂), ammonia (NH₃), nitrogen dioxide (NO₂) and
126 formaldehyde (HCHO).

127 [Based on the performance evaluation of the WRF-Chem simulations that indicate substantial](#)
128 [dry bias in the WRF60 simulations and large seasonality in the value-added by enhanced](#)
129 [resolution, we conducted two further year-long simulations at 60 km. In the first we held all](#)
130 [other simulation conditions constant but selected a different cumulus parameterization. In the](#)
131 [second, we held all simulation conditions constant but employed a different set of lateral](#)
132 [boundary conditions for the meteorology. In the context of the precipitation biases reported](#)
133 [herein it is worthy of note that discrepancies in simulated precipitation regimes are key](#)
134 [challenges in regional modelling \(both physical and coupled with chemistry\). Although the](#)
135 [Grell 3D scheme has been successfully applied in a number of prior analysis wherein the](#)
136 [model was applied at resolutions in the range of 1-36 km \(e.g. \(Grell and Dévényi,](#)
137 [2002;Lowrey and Yang, 2008;Nasrollahi et al., 2012;Sun et al., 2014;Zhang et al., 2016\)\), the](#)

138 [North American Regional Climate Change Assessment Program \(NARCCAP\) simulations](#)
 139 [with WRF at 50-km were also dry biased in the study domain \(Mearns et al., 2012\).](#) ~~(Mearns~~
 140 ~~et al., 2012)~~[Although there have been a number of studies that have sought to evaluate](#)
 141 [different cumulus schemes over different regions at different resolutions, no definitive](#)
 142 [recommendation has been made regarding the dependence of model's skill on resolution and](#)
 143 [cumulus parameterization](#) (Arakawa, 2004; Jankov et al., 2005; Nasrollahi et al., 2012; Li et al.,
 144 2014). [Thus, further research is needed to identify the optimal cumulus scheme for use over](#)
 145 [North America at coarser resolution. Thus, we performed a sensitivity analysis on the](#)
 146 [cumulus scheme at 60 km by applying the Grell-Freitas parameterization \(Grell and Freitas,](#)
 147 [2014\), which is the next generation of the Grell 3D scheme.](#)

148 **2 Materials and Methods**

149 **2.1 Spectral dependence of AOD**

150 Three properties dictate the actual aerosol direct radiative forcing: AOD, single scattering
 151 albedo and asymmetry factor, all of which are a function of the wavelength (λ) of incident
 152 radiation. The first property is related to the total columnar mass loading, typically dominates
 153 the variability of direct aerosol effect (Chin et al., 2009) and is the focus of the current
 154 research. The relationship between the aerosol size distribution and spectral dependence of
 155 AOD is described by a power law function:

$$156 \quad \beta(\lambda_1) = \beta(\lambda_2) \times \left(\frac{\lambda_1}{\lambda_2} \right)^{-\alpha} \quad (1)$$

157 where β is the particle extinction coefficient at a specific wavelength λ_1 —and α is the
 158 Ångström exponent (Ångström, 1964) which describes the wavelength dependence of AOD
 159 (and is inversely proportional to the average aerosol diameter):

$$160 \quad \alpha = \frac{\ln \frac{AOD(\lambda_1)}{AOD(\lambda_2)}}{\ln \frac{\lambda_2}{\lambda_1}} \quad (2)$$

161 The aerosol volume distribution ~~(and thus also its size distribution)~~ usually conforms to a
 162 multi-lognormal function with n modes:

$$163 \quad \frac{dV(r)}{d \ln r} = \sum_{i=1}^n \frac{C_i}{\sqrt{2\pi}\sigma_i} \exp\left[\frac{-(\ln r - \ln R_i)^2}{2\sigma_i^2}\right] \quad (3)$$

164 ~~Where~~ r is the particle radius and C_i , R_i and σ_i are the particle volume concentration, the
 165 geometric mean radius and the standard deviation in the mode i respectively.
 166 ~~, R_i is the geometric mean radius and σ_i is the geometric standard deviation, thus we~~
 167 have can thus compute AOD for a polydisperse distribution of aerosols with refractive index
 168 m in an atmospheric column of height Z as:

$$170 \quad AOD(\lambda) = \int \frac{3\beta(m, r, \lambda)}{4r} \frac{dV(r)}{d \ln r} d \ln r dZ \quad (4)$$

171 As indicated in (Schuster et al., 2006), “the spectral variability of extinction diminishes for
 172 particles larger than the incident wavelength”, thus fine mode particles contribute more to
 173 AOD in the visible ($\lambda \sim 0.5 \mu\text{m}$) than at longer wavelengths, whereas coarse mode particles
 174 provide a similar AOD both at short and long wavelengths. This is reflected in the Ångström
 175 parameter which can be thus used as a proxy for the fine mode fraction or fine mode radius
 176 (Schuster et al., 2006).

177 **2.2 WRF-Chem simulations**

178 WRF-Chem (version 3.6.1) simulations were performed for the calendar year 2008 over
 179 eastern North America, in a domain centered over southern Indiana (86°W , 39°N) at two
 180 resolutions, one close to the finest resolution designed for CMIP-6 global model runs (i.e. 60
 181 km, WRF60) and the other one at much higher resolution (12 km, WRF12). Simulation
 182 settings are identical for the two runs except for the time-step used for the physics (Table 1).
 183 Physical and chemical parameterizations were chosen to match previous work using WRF-
 184 Chem at 12 km on the same region which showed good performance relative to observations
 185 and the year 2008 was selected because it is representative of average climate and aerosol
 186 conditions during 2000 - 2014 (Crippa et al., 2016). More specifically the simulations
 187 adopted the RADM2 chemical mechanism (Stockwell et al., 1990) and a modal
 188 representation of the aerosol size distribution (MADE/SORGAM, (Ackermann et al.,
 189 1998; Schell et al., 2001)) with three lognormal modes and fixed geometric standard
 190 deviations (i.e. 1.7, 2 and 2.5 for Aitken, accumulation and coarse mode, respectively

191 (Ackermann et al., 1998;Grell et al., 2005)). Aerosol direct feedback was turned on and
192 coupled to the Goddard shortwave scheme (Fast et al., 2006). A telescoping vertical grid with
193 32 model layers from the surface to 50 hPa and 10 layers up to 800 hPa was selected.
194 Meteorological initial and boundary conditions from the North American Mesoscale Model at
195 12 km resolution ([NAM12](#)) are applied every 6 hours, while initial and chemical boundary
196 conditions are taken from MOZART-4 (Model for Ozone and Related chemical Tracers,
197 version 4) with meteorology from NCEP/NCAR-reanalysis (Emmons et al., 2010).
198 Anthropogenic emissions are specified for both WRF60 and WRF12 from the US National
199 Emission Inventory 2005 (NEI-05) (US-EPA, 2009) which provides hourly point and area
200 emissions at 4 km on 19 vertical levels. The simulation settings and specifically the use of a
201 modal representation of the aerosol size distribution were selected to retain computational
202 tractability. Accordingly, the 60 km simulations for the year 2008 completed in 6.4 hours
203 whereas the 12 km simulations completed in 9.5 days (230 hours) on the Cray XE6/XK7
204 supercomputer (Big Red II) owned by Indiana University, using 256 processors distributed
205 on 8 nodes.

206 [As described in detail below, in the WRF60 simulations configured as described in Table 1,](#)
207 [simulated precipitation during the summer months exhibits substantial dry bias, and the](#)
208 [analysis of value added by enhanced simulation resolution exhibited strong seasonality. We](#)
209 [performed a sensitivity analysis to the cumulus scheme, by conducting an additional year-](#)
210 [long simulation at 60 km using the Grell-Freitas parameterization \(Grell and Freitas, 2014\),](#)
211 [which is an evolution of Grell 3D that is scale-aware and treats some aspects of aerosol-cloud](#)
212 [interactions.](#)~~We performed a sensitivity analysis to the cumulus scheme, by conducting an~~
213 ~~additional year-long simulation at 60 km using the Grell-Freitas parameterization (Grell and~~
214 ~~Freitas, 2014), which is the next generation of the Grell 3D scheme.~~ We also tested the
215 [sensitivity of the simulation results to the meteorological boundary conditions, by repeating](#)
216 [the WRF60 simulations using output from the Global Forecast System \(GFS\) at 0.5°](#)
217 [resolution every 6 hours to provide the lateral boundary conditions.](#)

218 Value added is quantified [using Brier Skill Scores \(BSS\) and is evaluated in two ways: first](#)
219 [by evaluating the model performance as a function of simulation resolution and then using](#)
220 [climatology as the reference ‘forecast’.](#) In these analyses the ~~by degrading (averaging)~~ hourly
221 output from the 12 km resolution simulation [is degraded \(averaged\)](#) to 60 km (hereafter
222 WRF12-remap) as follows: the 12 km domain is resized excluding 2 grid cells at the border
223 to exactly match the 60 km resolution domain. Each coarse grid cell thus includes 5×5 12 km

224 resolution cells and its value is the mean of all valid 12 km grid cells inside it if at least half
225 of those cells contain valid AOD (i.e. no cloud cover), otherwise the whole coarse cell is
226 treated as missing. In all comparisons only cells with simultaneous (i.e. model and MODIS)
227 clear sky conditions are considered. A daily value from WRF-Chem is computed as an
228 instantaneous value for the hour nearest to the satellite overpass time. When the comparison
229 is done on a monthly basis, a monthly mean value is computed from the daily values obtained
230 under clear sky conditions, only if there are at least five valid observations in the month.

231 **2.3 Observations**

232 Model aerosol optical properties are evaluated relative to the MODIS Collection 6 dark-target
233 land aerosol product from aboard the Terra satellite (~1030 overpass local solar time (LST))
234 (Levy et al., 2013). To provide a consistent assessment of model skill, the evaluation of AOD
235 is conducted only on land areas since the MODIS dark-target ocean aerosol product is based
236 on a retrieval algorithm different from the one over land (Levy et al., 2013). Trace gas
237 concentrations are evaluated relative to measurements from the Ozone Monitoring Instrument
238 (OMI; version 3) (Chance, 2002) and the Infrared Atmospheric Sounding Interferometer
239 (IASI; NN version 1) (Whitburn et al., 2016) aboard the Aura (~1345 LST) and MetOp
240 satellites (~0930 LST), respectively. MODIS retrieves AOD at multiple λ including 470, 550,
241 and 660 nm, and the MODIS algorithm removes cloud-contaminated pixels prior to spatial
242 averaging over 10×10 km (at nadir). OMI and IASI have nadir resolutions of 13×24 km
243 and 12 km (circular footprint), respectively, and have been filtered to remove retrievals with
244 cloud fractions > 0.3 (Fioletov et al., 2011; McLinden et al., 2014; Vinken et al., 2014) and
245 OMI pixels affected by the row anomalies. MODIS, OMI, and IASI provide near daily global
246 coverage, although the row anomalies render portions of the OMI viewing swath unusable.
247 Uncertainty in AOD from MODIS is spatially and temporally variable. It has been estimated
248 as $\pm (0.05 + 15\%)$ for AOD over land (Levy et al., 2013), and prior research has reported
249 71% of MODIS Collection 5 retrievals fall within $0.05 \pm 20\%$ for AOD relative to
250 AERONET in the study domain (Hyer et al., 2011). The accuracy of OMI (“root sum of the
251 square of all errors, including forward model, inverse model, and instrument errors”
252 (Brinksma et al., 2003)) is 1.1 DU or 50% for SO_2 , $2 \times 10^{14} \text{ cm}^{-2}/30\%$ for
253 background/polluted NO_2 conditions, and 35% for HCHO. This uncertainty is typically
254 reduced by spatial and temporal averaging, as employed herein (Fioletov et al., 2011; Krotkov
255 et al., 2008). IASI NH_3 retrievals do not use an a priori assumption of emissions, vertical

256 distribution, or lifetime of NH_3 (i.e. no averaging kernel); therefore, NH_3 accuracy is variable
257 (Whitburn et al., 2016), and thus only retrievals with uncertainty lower than the retrieved
258 concentrations are used [herein](#) (~~Whitburn, et al. 2016~~).

259 For the model evaluation, satellite observations for each day are regridded to the WRF-Chem
260 discretization. This is done by averaging all valid retrievals within: 0.1° and 0.35° of the
261 WRF-Chem grid-cell center for the 12×12 km and 60×60 km resolutions, respectively for
262 MODIS; $0.125^\circ \times 0.18^\circ$ (along-track/latitudinal \times cross-track/longitudinal) and $0.365^\circ \times$
263 0.42° for OMI; 0.12° and 0.36° for IASI. To avoid issues from under-sampling, we require at
264 least 10 valid MODIS granules for the 60×60 km daily average to be computed and at least 5
265 daily averages to compute a monthly average for each grid cell. Model evaluation of gaseous
266 species is performed on a seasonal basis using standard scores (z-scores), which are
267 computed as the difference between the seasonal mean within a grid cell and the seasonal
268 spatial mean, divided by the seasonal spatial standard deviation. ~~The use of z-scores~~
269 ~~standard scores~~ allows comparison of the spatial patterns of satellite observations and model
270 output in terms of standard deviation units from the mean.

271 The simulated meteorological properties are evaluated using Modern-Era Retrospective
272 analysis for Research and Applications (MERRA-2) reanalysis data as the target. MERRA-2
273 is a homogenized and continuous in time description of atmospheric properties on a 3-
274 dimensional global grid (horizontal resolution of $0.5^\circ \times 0.625^\circ$, L72), developed by NASA and
275 was released in Fall 2015 (Molod et al., 2015). MERRA-2 provides hourly values of T_{2m} and
276 $PBLH$, and vertical profile of 3-dimensional variables every 3 hours on a large number of
277 pressure levels. Here we compute the total specific humidity (Q_{PBL}) of the lowest 8 pressure
278 levels (i.e. in the boundary-layer approximated as the layer from 1000 to 825 hPa) in
279 MERRA-2, assuming an average air density in the PBL of 1.1 kg m^{-3} . For the evaluation of
280 simulated precipitation, we use accumulated monthly total values.

281 **2.4 Quantification of model performance and added-value**

282 Taylor diagrams summarize three aspects of model performance relative to a reference: the
283 spatial correlation coefficient (i.e. Pearson correlation of the fields, r), the ratio of spatial
284 standard deviations of the two spatial fields ($\sigma_{\text{wrf}}/\sigma_{\text{sat}}$) and the root mean squared difference
285 (Taylor, 2001). Here Taylor diagrams are presented for monthly mean AOD from WRF60,
286 WRF12 and WRF12-remap relative to MODIS at different wavelengths (Fig. 1 d-f). Because
287 AOD is not normally distributed, Spearman's rank correlation coefficients (ρ) of the mean

288 monthly AOD spatial fields are also computed to reduce the impact of a few outliers and the
 289 small sample size during cold months (Table 2). To assess the significance of ρ while
 290 accounting for multiple testing, we apply a Bonferroni correction (Simes, 1986) in which for
 291 m hypothesis tests, the null hypothesis is rejected if $p \leq \frac{\alpha}{m}$, where p is the p-value and α is
 292 the confidence level (0.05 is used here).

293 We further quantify the value added (or lack of thereof) of the high-resolution simulations
 294 using the following metrics:

295 **(i) Brier Skill Score**

296 The primary metric used to quantify the added value of WRF12-remap versus WRF60 is the
 297 Brier Skill Score (BSS) (Murphy and Epstein, 1989):

$$298 \quad BSS = \frac{r_{F'P'}^2 - \left(r_{F'P'} - \frac{\sigma_{F'}}{\sigma_{P'}} \right)^2 - \left(\frac{\langle P' \rangle - \langle F' \rangle}{\sigma_{P'}} \right)^2 + \left(\frac{\langle P' \rangle}{\sigma_{P'}} \right)^2}{1 + \left(\frac{\langle P' \rangle}{\sigma_{P'}} \right)^2} \quad (5)$$

299 where F is the “forecast” (i.e. the 12 km simulations mapped to 60 km, WRF12-remap); P is
 300 the “target” (i.e. MODIS at 60 km) and output from WRF60 are used as the reference
 301 forecast; F' the difference between 12 km estimates regridded to 60 km and MODIS; P' the
 302 difference between the 60 km simulation and MODIS. [In the analysis of BSS relative to the
 303 long-term \(15-year\) climatology from MODIS, the monthly mean climatological value of
 304 AOD is used as the target reference forecast, while WRF60 and WRF12-remap are used as the
 305 forecasts, and monthly mean AOD from MODIS at 60 km is the target.-](#)

306 BSS measures [by](#) how much a test simulation (i.e. WRF12-remap) more closely (or poorly)
 307 reproduces observations (from MODIS, MERRA-2 or other satellite products) relative to a
 308 control (WRF60) run. [For example, a](#) BSS > 0 indicates WRF12, even when regridded to 60
 309 km, does add value. The first term in (5) ranges from 0 to 1, is described as the potential skill,
 310 and is the square of the spatial correlation coefficient between forecast and reference
 311 anomalies to MODIS. It is the skill score achievable if both the conditional bias (second
 312 term) and overall bias (third term) were zero, and for most of the variables considered herein
 313 (particularly AOD) it contributes to a positive BSS in most calendar months (and seasons).
 314 The second term (the conditional bias, > 0), is the square of the difference between the
 315 anomaly correlation coefficient and the ratio of standard deviation of the anomalies and is

316 small if for all points F' is linear to P' . The third term is referred to as the forecast anomaly
317 bias, and is the ratio of the difference between the mean anomalies of WRF12-remap and the
318 observations relative to WRF60 and the standard deviation of WRF60 anomaly relative to
319 observed values. The fourth term is the degree of agreement and appears in both the
320 numerator and denominator. It is computed as the square of the ratio of the mean anomaly
321 between WRF60 and observations and the standard deviation of the anomalies.

322 **(ii) Pooled paired t-test**

323 To identify which areas in space contribute most to the added value, we compare daily mean
324 AOD fields from WRF-Chem at different resolutions and MODIS. We perform a pooled
325 paired t-test to evaluate the null hypothesis that those differences come from normal
326 distributions with equal means and equal but unknown variances (the test statistic has a
327 Student's t distribution with $df = n + m - 2$, and the sample standard deviation is the pooled
328 standard deviation, where n and m are the two sample sizes). The test is conducted by
329 climatological season (e.g. winter = DJF) since there are fewer than 20 valid AOD
330 observations in most 60 km grid cells for each calendar month (Fig. 2). Given the large
331 number of hypothesis tests performed (i.e. one for each 60 km grid cell), we adjust the p-
332 values using the False Discovery Rate (FDR) approach (Benjamini and Hochberg, 1995). In
333 this approach, p-values from the t-tests are ranked from low to high (p_1, p_2, \dots, p_m), then the
334 test with the highest rank, j , satisfying:

$$335 \quad p_j \leq \frac{j}{m} \alpha \quad (6)$$

336 is identified. Here all p-values satisfying Eq. 6 with $\alpha=0.1$ are considered significant.

337 **(iii) Accuracy and Hit Rate in identification of extremes**

338 For each month we identify grid cells in which the wavelength specific AOD exceeds the 75th
339 percentile value computed from all grid cells and define that as an extreme. Thus grid cells
340 with extreme AOD are independently determined for MODIS and WRF-Chem at different
341 resolutions. The spatial coherence in identification of extremes in the fields is quantified
342 using two metrics: the *Accuracy* and the *Hit Rate (HR)*. The *Accuracy* indicates the overall
343 spatial coherence and is computed as the number of grid cells co-identified as extreme and
344 non-extreme between WRF-Chem and MODIS relative to the total number of cells with valid
345 data. The *HR* weights only correct identification of extremes in MODIS by WRF-Chem.

346 **3 Results**

347 **3.1 Quantifying the value added of increased spatial resolution**

348 When WRF-Chem is applied at 60 km resolution the degree of association of the resulting
349 spatial fields of mean monthly AOD at the three wavelengths with MODIS varies seasonally.
350 Smallest RMSD and highest Spearman spatial correlations (ρ) with MODIS observations
351 generally occur during months with highest mean AOD (i.e. during summer, Fig. 1 d-f and
352 Fig. 3), and reach a maximum in August ($\rho = 0.60$, Table 2). However, while the patterns of
353 relative AOD variability are well captured, the absolute magnitudes and spatial gradients of
354 AOD during the summer are underestimated by WRF60 (Fig. 1 d-f and Fig. 3, Table S1).
355 High spatial correlations ($\rho > 0.40$) are also observed in March, April and November (Table
356 2), when the ratio of spatial standard deviations is closer to 1 (Fig. 1 d-f, Table S1). Only a
357 weak wavelength dependence is observed in the performance metrics as described on Taylor
358 diagrams. The spatial variability is generally more negatively biased for AOD at 660 nm
359 (Table S1), indicating that WRF60 simulations tend to produce larger diameter aerosols
360 homogeneously distributed over the domain, whereas MODIS observations indicate more
361 spatial variability.

362 The performance of WRF60 simulations relative to MODIS contrasts with analyses of
363 WRF12 and WRF12-remap. WRF12 and WRF12-remap indicate highest spatial correlations
364 with MODIS observations throughout the summer months ($\rho = 0.5-0.7$, Table 2), although
365 the bias towards simulation of more coarse aerosols than are observed is consistent across the
366 two simulations and with prior research (see details provided in (Crippa et al., 2016)).
367 However, simulations at 12 km (WRF12) show positive ρ with MODIS for all λ in all
368 calendar months, while mean monthly spatial fields of AOD from WRF60 show low and/or
369 negative correlations with MODIS during May, June, September, October and December,
370 indicating substantial differences in the degree of correspondence with MODIS AOD in the
371 two simulations, and higher fidelity of the enhanced resolution runs (Tables 2 and S1).

372 Monthly mean spatial fields of AOD(λ) as simulated by WRF12 or WRF12-remap exhibit
373 positive Spearman correlation coefficients (ρ) with MODIS observations for all calendar
374 months and range from ~ 0.25 for WRF12-remap (0.20 for WRF12) during winter to ~ 0.70
375 and 0.64, respectively during summer (Table 2). Spearman's ρ are uniformly higher in
376 WRF12-remap than WRF12 indicating a mismatch in space in the high-resolution simulation
377 (i.e. that grid cells with high AOD are slightly displaced in the 12 km simulations possibly

378 due to the presence of sub-grid scale aerosol plumes (Rissman et al., 2013)). Mean monthly
379 fields of AOD (all λ) from both WRF12 and WRF12-remap exhibit lower ρ with MODIS in
380 February-April and November than the 60 km runs (Table 2). These discrepancies appear to
381 be driven by conditions in the south of the domain. For example, differences between
382 WRF60/WRF12-remap vs. MODIS during all seasons are significant according to the paired
383 t-test over Florida and along most of the southern coastlines (Fig. 2). This region of
384 significant differences extends up to $\sim 40^\circ\text{N}$ during summer and fall, reflecting the stronger
385 north-south gradient in AOD from MODIS and WRF12-remap that is not captured by
386 WRF60 (see example for $\lambda = 550$ nm, Fig. 3). These enhancements in the latitudinal
387 gradients from WRF12-remap are also manifest in the physical variables (particularly
388 specific humidity as discussed further below).

389 The differences in the absolute values of mean monthly AOD deriving from differences in the
390 resolution at which WRF-Chem was applied are of sufficient magnitude (a difference of up to
391 0.2 in regions with a mean AOD value of 0.4), particularly in the summer months (Fig. 4), to
392 raise concerns. However, detailed investigation of the simulations settings and repetition of
393 the 60 km simulation resulted in virtually identical results indicating no fault can be found in
394 the analysis. Further, we note that the eastern-half of North America was also identified as a
395 region of high discrepancy in global ESM (Myhre et al., 2013a).

396 To further investigate differences in the simulation output due to spatial discretization we
397 computed Brier Skill Scores (BSS). In this analysis AOD for each λ from WRF12-remap are
398 used as the ‘forecast’, output from WRF60 are used as the reference forecast and MODIS
399 observations at 60 km are used as the target. ~~Despite effects of the boundary conditions
400 appear in some variables (e.g. in Fig. 4 and Figs. S1-S3), the BSS results do not significantly
401 change even when those cells are removed from the analysis.~~ BSS exceed 0 during all months
402 except for September and October, and largest BSS (> 0.5) for AOD (all λ) is found during
403 most months between December and July (Fig. 5a-c). This indicates that running WRF-Chem
404 at 12 km resolution adds value relative to WRF60, even when the WRF12 output is remapped
405 to 60 km. BSS do not strongly depend on λ , indicating the added value from enhanced
406 resolution similarly affects particles of different sizes. Inspecting the terms defining the BSS
407 provides information about the origin of the added value (Fig. 5a-c). The positive BSS
408 derives principally from the potential skill (first term in Eq. 5), which demonstrates a
409 reduction in bias and/or more accurate representation of the spatial gradients in WRF12-

410 remap. This term exhibits weak seasonality with values below 0.5 only during August and
411 fall months. The second and third terms are close to zero during most months, although
412 bigger biases are found during August-October. The substantial conditional bias during late
413 summer and early fall is the result of the large ratio of standard deviations (> 1 , i.e. the spatial
414 variability of the anomaly relative to MODIS is larger for WRF12-remap than WRF60, Table
415 S1). It thus contributes to the negative BSS found in September and October, which are also
416 identified as outlier months in WRF12-remap from the Taylor diagram analysis (Fig. 1).
417 Output for these months show modest spatial correlations with MODIS and higher ratio of
418 standard deviations than in WRF60-MODIS comparisons (Fig. 1, Table S1). Previous work
419 showed that the lower model skill (in WRF12) during September and October may be
420 partially attributable to a dry bias in precipitation from WRF-Chem relative to observations.
421 As a result, simulated AOD and near-surface aerosol nitrate and sulfate concentrations are
422 positively biased over large parts of the domain (Crippa et al., 2016). Although the effects of
423 the boundary conditions appear in some variables (e.g. in Fig. 4 and Figs. S1-S3), the BSS
424 results do not significantly change even when those cells are removed from the analysis.

425 When the BSS is used to assess the skill of each model relative to MODIS AOD
426 climatological mean over the years 2000-2014, WRF12-remap is found to add value relative
427 to the climatology (i.e. BSS > 0) during summer months and Nov-Jan whereas BSS for
428 WRF60 is positive from late Fall to early Spring (Fig. 5d). The fact that WRF-Chem does not
429 always outperform the climatology is expected since the model is based on time invariant
430 emissions and skills are assessed relative to a year selected to be representative of the AOD
431 climatology. Mean seasonal AOD from MODIS retrievals over the study region during 2008
432 lie within ± 0.2 standard deviations of the climatology (Crippa et al., 2016).the AOD Mean
433 seasonal AOD from MODIS retrievals over the study region during 2008 lie within ± 0.2
434 standard deviations of the climatology (Crippa et al., 2016). Interestingly, BSS for most
435 months (excluding September) are higher for the WRF60 simulations conducted using lateral
436 boundary conditions from NAM12 than GFS.~~We also tested the internal variability of the~~
437 ~~model by driving it with meteorological boundary conditions from the Global Forecast~~
438 ~~System (GFS) at 0.5 degree resolution every 6 hours, and drawn analogous conclusions to~~
439 ~~those derived from the aforementioned runs.~~

440 Model resolution also affects the *Accuracy* and *Hit Rate (HR)* for identification of areas of
441 extreme AOD (AOD $> 75^{\text{th}}$ percentile). Highest coherence in the identification of extreme
442 AOD in space identified in WRF12-remap (and WRF12) relative to MODIS is found during

443 May-August ($HR = 53-77\%$) vs. WRF60 ($HR = 17-54\%$, Table 3). Conversely highest HR are
444 found for WRF60 and MODIS during winter and early spring, and indeed exceed those for
445 WRF12 and WRF12-remap (Table 3, e.g. Feb: $HR = 0.78$ for WRF60, and 0.67 and 0.68 for
446 WRF12 and WRF12-remap, respectively). These differences are consistent with the
447 observation that WRF12-remap overestimates the scales of AOD coherence and AOD
448 magnitude during the cold season along coastlines and over much of the domain in April
449 (Fig. 3).

450 The synthesis of these analyses is thus that the higher resolution simulation increases the
451 overall spatial correlation, decreases overall bias in AOD close to the peak of the solar
452 spectrum relative to MODIS observations and therefore the higher-resolution simulations
453 better represent aerosol direct climate forcing. However, WRF12-remap exhibits little
454 improvement over WRF60 in terms of reproducing the spatial variability of AOD in the
455 visible wavelengths and further that WRF12-remap tends to be more strongly positively
456 biased in terms of mean monthly AOD outside of the summer months (Fig. 2 and Fig. 3).
457 Also the improvement in detection of areas of extreme AOD in the higher resolution
458 simulations (WRF12-remap) is manifest only during the warm season.

459 **3.2 Investigating the origin of the added value and sources of error in simulated AOD**

460 As documented above, WRF-Chem applied at either 60 or 12 km resolution over eastern
461 North America exhibits some skill in reproducing observed spatial fields of AOD and the
462 occurrence of extreme AOD values. However, marked discrepancies both in space and time
463 are found, and at least some of them show a significant dependence on model resolution.
464 Thus, we investigated a range of physical conditions and gas phase concentrations known to
465 be strongly determinant of aerosol dynamics in terms of the BSS as a function of model
466 resolution and also in terms of the mean monthly spatial patterns.

467 WRF12 even when remapped to 60 km provides more accurate description of key
468 meteorological variables such as specific humidity (Q) within the boundary layer, $PBLH$,
469 surface temperature and precipitation (see Fig. 6, S1, S2 and S3) when compared to MERRA-
470 2, as indicated by the positive BSS during almost all months (Fig. 7a). Good qualitative
471 agreement is observed for the spatial patterns and absolute magnitude of T_{2m} in both WRF60
472 and WRF12-remap relative to MERRA-2 for all seasons (Fig. S1) leading to only modest
473 magnitude of BSS (i.e. value added by the higher resolution simulations (Fig. 7a)). The
474 aerosol size distribution and therefore wavelength specific AOD exhibits a strong sensitivity

475 to Q (Santarpia et al., 2005) due to the presence of hygroscopic components in atmospheric
476 aerosols and thus the role of water uptake in determining aerosol diameter, refractivity and
477 extinction coefficient (Zieger et al., 2013). For example, the hygroscopic growth factor,
478 which indicates the change of aerosol diameter due to water uptake, is ~ 1.4 for pure
479 ammonium sulfate with dry diameter of 532 nm at relative humidity of 80%, thus biases in
480 representation atmospheric humidity may lead to big errors in simulated aerosol size and
481 AOD (Flores et al., 2012). Our previous analyses of the 12 km resolution simulations
482 indicated overestimation of sulfate aerosols (a highly hygroscopic aerosol component, and
483 one which in many chemical forms exhibits strong hysteresis (Martin et al., 2004)) relative to
484 observed near-surface $PM_{2.5}$ concentrations during all seasons except for winter (Crippa et al.,
485 2016), leading to the hypothesis that simulated AOD and discrepancies therein may exhibit a
486 strong dependence on Q . Consistent with that postulate, Q_{PBL} from WRF12-remap exhibits a
487 moist bias in cloud-free grid cells mostly during warm months, whereas WRF60 is
488 characterized by a dry bias during all seasons (Fig. 6). Despite the positive bias, WRF12-
489 remap better captures the seasonal spatial patterns of Q_{PBL} in MERRA-2, leading to positive
490 BSS in all calendar months. Thus, there is added value by higher-resolution simulations in
491 representation of one of the key parameters dictating particle growth and optical properties.
492 Spatial patterns of differences in Q_{PBL} from WRF60 and WRF12-remap relative to MERRA-
493 2 (Fig. 6) exhibit similarities to differences in AOD (Fig. 4). WRF60 is dry-biased relative to
494 WRF12 particularly during the summer (and fall) and underestimates Q_{PBL} relative to
495 MERRA-2 during all seasons over the southern states and over most of continental US during
496 summer and fall. Conversely, WRF12-remap overestimates Q_{PBL} over most of continental US
497 during summer and fall relative to MERRA-2.

498 $PBLH$ is a key variable for dictating near-surface aerosol concentrations but is highly
499 sensitive to the physical schemes applied, and biases appear to be domain and resolution
500 dependent. However, this parameter is comparatively difficult to assess because differences
501 in $PBLH$ from WRF-Chem and MERRA-2 may also originate from the way they are
502 computed (i.e. from heat diffusivity in MERRA-2 (Jordan et al., 2010) and from turbulent
503 kinetic energy in WRF-Chem (Janjić, 2002; von Engeln and Teixeira, 2013)). Nevertheless,
504 the Mellor-Yamada-Janjich PBL scheme combined with the Noah Land Surface Model
505 applied in this work was found to produce lower PBL heights (Zhang et al., 2009) than other
506 parameterizations. Thus, the positive bias in simulated AOD and surface $PM_{2.5}$ concentrations
507 (reported previously in (Crippa et al., 2016)) may be linked to the systematic underestimation

508 of *PBLH* simulated by WRF12-remap over continental US relative to MERRA-2 during all
509 seasons (except winter) with greatest bias over regions of complex topography (Fig. S2). A
510 positive bias (of several hundred meters) in terms of *PBLH* for WRF simulations using the
511 MYJ parameterization was previously reported for high-resolution simulations over complex
512 terrain (Rissman et al., 2013), and a positive bias in *PBLH* is also observed in the 60 km
513 simulations presented herein (Fig. S2). This may provide a partial explanation for the strong
514 negative bias in AOD in WRF60 during summer (Fig. 3). In general, the BSS indicate
515 improvement in the simulation of *PBLH* in WRF12-remap than in WRF60 (Fig. 7a).

516 ~~————— Aerosol concentrations (and thus AOD) are dependent on aerosol residence times, and
517 thus the source and sink time scales. Analysis of sixteen global models from the AeroCom
518 project indicate wet scavenging is the dominant sink term for the predominant aerosol species
519 (sulfate and particulate organic matter; ammonium and nitrates not evaluated in study) in the
520 study area (Hand et al., 2012; Textor et al., 2006) Thus, the low precipitation bias in WRF60
521 simulations should result in a high AOD bias, but may also lead to poor representation of
522 surface moisture availability, boundary layer humidity, and ultimately aerosol water content.
523 High model to model discrepancy has been found in simulating aerosol water uptake (Textor
524 et al., 2006).~~

525 Consistent with the dry bias in Q_{PBL} in WRF60, total accumulated precipitation is also
526 underestimated in WRF60, while WRF12-remap captures the absolute magnitudes and the
527 spatial patterns therein (Fig. S3). Analysis of hourly precipitation rates also showed higher
528 skill of WRF12-remap than WRF60 in correctly simulating precipitation occurrence (*HR*)
529 relative to MERRA-2 (Table S2). More specifically WRF12-remap correctly predicts
530 between 40% and 70 % of precipitation events in MERRA-2 with highest skill during winter
531 months, whereas WRF60 output exhibits lower HR (~6% during summer and 30% during
532 winter). This result thus confirms our expectation of a strong sensitivity of model
533 performance to resolution due to the inherent scale dependence in the cumulus scheme.
534 ~~Precipitation biases are key challenges in regional modelling (both physical and coupled with
535 chemistry). For example, the North American Regional Climate Change Assessment Program
536 (NARCCAP) simulations with WRF at 50 km were also dry biased in the study domain.
537 Although there have been a number of studies that have sought to evaluate different cumulus
538 schemes over different regions at different resolutions, no definitive recommendation has
539 been made regarding the dependence of model's skill on resolution and cumulus
540 parameterization (Arakawa, 2004; Jankov et al., 2005; Nasrollahi et al., 2012). A strong~~

541 ~~sensitivity on the adopted cumulus scheme was found in (Li et al., 2014), where the Grell 3~~
542 ~~scheme is responsible for a wet bias in the Southeast US (mostly in summer). In that study~~
543 ~~the model was run at 15 km resolution which the authors identified as the minimum~~
544 ~~resolution to be able to resolve the rainfall system with a 60 km spatial scale typical of the~~
545 ~~region. Further, the Grell 3D[PP1] scheme was successfully applied at resolutions in the~~
546 ~~1–36 km (e.g. (Grell and Dévényi, 2002; Lowrey and Yang, 2008; Nasrollahi et al., 2012; Sun~~
547 ~~et al., 2014; Zhang et al., 2016)), although further research is needed to identify the optimal~~
548 ~~cumulus scheme over North America at coarser resolution. We performed a sensitivity~~
549 ~~analysis on the cumulus scheme at 60 km by applying the Grell-Freitas parameterization~~
550 ~~(Grell and Freitas, 2014), which is the next generation of the Grell 3D scheme. Analysis of~~
551 ~~precipitation seasonal fields—Use of the Grell-Freitas parameterization in the WRF60~~
552 ~~simulations did not lead to substantially different do not show significant differences in~~
553 ~~magnitude and/or spatial patterns of precipitation compared to WRF60 adopting applied with~~
554 ~~the Grell 3D scheme, and no improvement in agreement with output from MERRA2. As a~~
555 ~~result, also the BSS of both precipitation and AOD at different wavelengths lead to the same~~
556 ~~conclusions on the higher performance of WRF12-remap vs WRF60. –The findings of a~~
557 ~~negative bias in WRF60 simulations without a corresponding overestimation of AOD may~~
558 ~~appear counter-intuitive since aerosol concentrations (and thus AOD) are dependent on~~
559 ~~aerosol residence times and analyses of sixteen global models from the AeroCom project~~
560 ~~indicate wet scavenging is the dominant removal process for most aerosol species in the study~~
561 ~~area (Hand et al., 2012; Textor et al., 2006). However, the negative precipitation bias in~~
562 ~~WRF60 simulations appears to be linked to poor representation of surface moisture~~
563 ~~availability, boundary layer humidity (Fig. 6), and ultimately aerosol water content (and~~
564 ~~hence AOD). We also tested the internal variability of the model by driving it with~~
565 ~~meteorological boundary conditions from the Global Forecast System (GFS) at 0.5 degree~~
566 ~~resolution every 6 hours, and drawn analogous conclusions to those derived from the~~
567 ~~aforementioned runs.~~

568
569 Gas phase concentrations (transformed into z-scores) from WRF12-remap show higher
570 agreement with satellite observations during almost all months, as indicated by the positive
571 BSS (Fig. 7b). However given the limited availability of valid satellite observations
572 (especially during months with low radiation intensity), the BSS are likely only robust for the
573 summer months for all species. Nevertheless, with the exception of NH₃ during June, BSS for

574 all months are above or close to zero indicating that on average, the enhanced resolution
575 simulations do improve the quality of the simulation of the gas phase species even when
576 remapped to 60 km resolution. Further, the seasonal average spatial patterns of the total
577 columnar concentrations, expressed in terms of z-scores, also exhibit qualitative agreement
578 with the satellite observations (Fig. S4-S7).

579 **4 Concluding remarks**

580 This analysis is one of the first to quantify the impact of model spatial resolution on the
581 spatio-temporal variability and magnitude of AOD, and does so using simulations for a full
582 calendar year. Application of WRF-Chem at two different resolutions (60 km and 12 km)
583 over eastern North America for a representative year (2008) leads to the following
584 conclusions:

- 585 - Higher resolution simulations add value (i.e. enhance the fidelity of AOD at and near
586 to the peak in the solar spectrum) relative to a coarser run, although the improvement
587 in model performance is not uniform in space and time. Brier Skill Scores for the
588 remapped simulations (i.e. output from simulations conducted at 12 km (WRF12)
589 then averaged to 60 km, WRF12-remap) are positive for ten of twelve calendar months,
590 and for AOD($\lambda=550$ nm) exceed 0.5 for seven of twelve months.
- 591 - Spatial correlations of output from WRF12 and WRF12-remap with observations
592 from MODIS are higher than output from a simulation conducted at 60 km during
593 most months. For example, in contrast to WRF-Chem simulations at 60 km (WRF60),
594 simulations conducted at 12 km (WRF12) show positive spatial correlations with
595 MODIS for all λ in all calendar months, and particularly during summer ($\rho = 0.5-0.7$).
- 596 - Output from WRF12 and WRF12-remap exhibit highest accord with MODIS
597 observations in capturing the frequency, magnitude and location of extreme AOD
598 values during summer when AOD is typically highest. During May-August WRF12-
599 remap has *Hit Rates* for identification of extreme AOD of 53-78%.
- 600 ~~At least some of the improvement in the accuracy with which AOD is reproduced in~~
601 ~~the higher resolution simulations may be due to improved fidelity of specific humidity~~
602 ~~and thus more accurate representation of hygroscopic growth of some aerosol~~
603 ~~components.~~
- 604 - Higher-resolution simulations also add value in the representation of other key
605 meteorological variables such as temperature, boundary layer height and precipitation.

606 Both spatial patterns and precipitation occurrence are better captured by WRF12-
607 remap.

608 - At least some of the improvement in the accuracy with which AOD is reproduced in
609 the higher resolution simulations may be due to improved fidelity of specific humidity
610 and thus more accurate representation of hygroscopic growth of some aerosol
611 components.

~~612 Aerosol concentrations (and thus AOD) are dependent on aerosol residence times, and
613 thus the source and sink time scales. Analysis of sixteen global models from the
614 AeroCom project indicate wet scavenging is the dominant sink term for the
615 predominant aerosol species (sulfate and particulate organic matter; ammonium and
616 nitrates not evaluated in study) in the study area (Hand et al., 2012; Textor et al., 2006).
617 Thus, the low precipitation bias in WRF60 simulations should result in a high AOD
618 bias, but may also lead to poor representation of surface moisture availability,
619 boundary layer humidity, and ultimately aerosol water content. High model to model
620 discrepancy has been found in simulating aerosol water uptake (Textor et al., 2006).~~

621 - More accurate representation of spatial patterns and magnitude of gaseous species that
622 play a key role in particle formation and growth is also achieved by running WRF-
623 Chem at high resolution.

624 It is worthy of note that even the 12 km resolution WRF-Chem simulations exhibit substantial
625 differences in AOD relative to MODIS over eastern North America, and the agreement varies
626 only slightly with wavelength. This may be partially attributable to use of the modal approach
627 to represent the aerosol size distribution in order to enhance computational tractability. In this
628 application each mode has a fixed geometric standard deviation (σ_g), which can lead to biases
629 in simulated AOD in the visible wavelengths by up to 25% (Brock et al., 2016) (with the
630 model overestimating observations if the prescribed σ_g is larger than the observed one).
631 Setting $\sigma_g = 2$ for the accumulation mode (the default in WRF-Chem) may lead to an
632 overestimation of the number of particles at the end of the accumulation mode tail, and there
633 is evidence that a value of $\sigma_{g,acc}=1.40$ leads to higher agreement with observations (Mann et
634 al., 2012). Further possible sources of the AOD biases reported herein derive from selection
635 of the physical schemes (e.g. planetary boundary layer (*PBL*) schemes and land-surface
636 model (Misenis and Zhang, 2010; Zhang et al., 2009)). Further, it is worth mentioning that
637 NEI emissions are specified based on an average summertime weekday, so enhanced model
638 performance might be achieved if seasonally varying emissions were available. [Future work](#)

639 ~~will include a systematic sensitivity analysis of these effects.~~ Naturally, there is a need for
640 more research regarding the sensitivity of WRF-Chem simulations of climate relevant aerosol
641 properties to the parameterizations used, the lateral boundary conditions employed and the
642 resolution at which the simulations are conducted.

643 **Acknowledgments**

644 This research was supported in part by a L'Oréal-UNESCO UK and Ireland Fellowship For
645 Women In Science (to PC), the Natural Environmental Research Council (NERC) through
646 the LICS project (ref. NE/K010794/1), grants to SCP from US NSF (grant # 1517365) and
647 NASA (NNX16AG31G), and a NASA Earth and Space Science Fellowship Program - Grant
648 "14-EARTH14F-0207" (to RCS). Further support was provided by the Lilly Endowment,
649 Inc., through its support for the Indiana University Pervasive Technology Institute and the
650 Indiana METACyt Initiative. We gratefully acknowledge the NASA scientists responsible for
651 MERRA-2 and MODIS products, the developers of WRF-Chem, and Lieven Clarisse, Simon
652 Whitburn, and Martin Van Damme for producing and sharing the NH₃ retrievals. The clarity
653 and content of this manuscript was substantially improved by the comments of three
654 reviewers.

656 **References**

- 657 Ackermann, I. J., Hass, H., Memmesheimer, M., Ebel, A., Binkowski, F. S., and Shankar, U.:
658 Modal aerosol dynamics model for Europe: development and first applications, Atmospheric
659 Environment, 32, 2981-2999, [http://dx.doi.org/10.1016/S1352-2310\(98\)00006-5](http://dx.doi.org/10.1016/S1352-2310(98)00006-5), 1998.
- 660 Anderson, T. L., Charlson, R. J., Winker, D. M., Ogren, J. A., and Holmén, K.: Mesoscale
661 Variations of Tropospheric Aerosols, Journal of the Atmospheric Sciences, 60, 119-136, doi:
662 [http://dx.doi.org/10.1175/1520-0469\(2003\)060<0119:MVOTA>2.0.CO;2](http://dx.doi.org/10.1175/1520-0469(2003)060<0119:MVOTA>2.0.CO;2), 2003.
- 663 Ångström, A.: The parameters of atmospheric turbidity, Tellus, 16, 64-75, 10.1111/j.2153-
664 3490.1964.tb00144.x, 1964.
- 665 Arakawa, A.: The Cumulus Parameterization Problem: Past, Present, and Future, Journal of
666 Climate, 17, 2493-2525, doi:10.1175/1520-0442(2004)017<2493:RATCPP>2.0.CO;2, 2004.
- 667 Benjamini, Y., and Hochberg, Y.: Controlling the False Discovery Rate: A Practical and
668 Powerful Approach to Multiple Testing, Journal of the Royal Statistical Society. Series B
669 (Methodological), 57, 289-300, 1995.
- 670 Boucher, O., D. Randall, P. Artaxo, C. Bretherton, G. Feingold, P. Forster, V.-M. Kerminen,
671 Y. Kondo, H. Liao, U. Lohmann, P. Rasch, S.K. Satheesh, S. Sherwood, B. Stevens and X.Y.

- 672 Zhang: Clouds and Aerosols, in: Climate Change 2013: The Physical Science Basis.
673 Contribution of Working Group I to the Fifth Assessment Report of the Intergovernmental
674 Panel on Climate Change, edited by: Stocker, T. F., D. Qin, G.-K. Plattner, M. Tignor, S.K.
675 Allen, J. Boschung, A. Nauels, Y. Xia, V. Bex and P.M. Midgley, Cambridge University
676 Press, Cambridge, United Kingdom and New York, NY, USA, 33–115, 2013.
- 677 Brinksma, E. J., Boersma, K. F., Levelt, P. F., and McPeters, R. D.: OMI validation
678 requirements document, Version 1, Rep. RS-OMIE-KNMI-345, 66, 2003.
- 679 Brock, C. A., Wagner, N. L., Anderson, B. E., Attwood, A. R., Beyersdorf, A., Campuzano-
680 Jost, P., Carlton, A. G., Day, D. A., Diskin, G. S., Gordon, T. D., Jimenez, J. L., Lack, D. A.,
681 Liao, J., Markovic, M. Z., Middlebrook, A. M., Ng, N. L., Perring, A. E., Richardson, M. S.,
682 Schwarz, J. P., Washenfelder, R. A., Welti, A., Xu, L., Ziemba, L. D., and Murphy, D. M.:
683 Aerosol optical properties in the southeastern United States in summer – Part 1: Hygroscopic
684 growth, *Atmospheric Chemistry and Physics*, 16, 25695-25738, doi:10.5194/acp-16-5009-
685 2016, 2016.
- 686 Chance, K.: OMI algorithm theoretical basis document, volume IV: OMI trace gas
687 algorithms, 2002.
- 688 Chen, F., and Dudhia, J.: Coupling an advanced land surface–hydrology model with the Penn
689 State–NCAR MM5 modeling system. Part I: model implementation and sensitivity, *Monthly*
690 *Weather Review*, 129, 569-585, doi:10.1175/1520-
691 0493(2001)129<0569:CAALSH>2.0.CO;2, 2001.
- 692 Chin, M., Kahn, R. A., and Schwartz, S. E.: Atmospheric Aerosols Properties and Climate
693 Impacts. A Report by the U.S. Climate Change Science Program and the Subcommittee on
694 Global Change Research, in, National Aeronautics and Space Administration, Washington,
695 D.C., USA, 128, 2009.
- 696 Crippa, P., Sullivan, R. C., Thota, A., and Pryor, S. C.: Evaluating the skill of high-resolution
697 WRF-Chem simulations in describing drivers of aerosol direct climate forcing on the regional
698 scale, *Atmospheric Chemistry and Physics*, 16, 397-416, 10.5194/acp-16-397-2016, 2016.
- 699 Di Luca, A., de Elía, R., and Laprise, R.: Challenges in the Quest for Added Value of
700 Regional Climate Dynamical Downscaling, *Curr Clim Change Rep*, 1, 10-21,
701 10.1007/s40641-015-0003-9, 2015.
- 702 Diaconescu, E., and Laprise, R.: Can added value be expected in RCM-simulated large
703 scales?, *Climate Dynamics*, 41, 1769-1800, 10.1007/s00382-012-1649-9, 2013.
- 704 Emmons, L. K., Walters, S., Hess, P. G., Lamarque, J. F., Pfister, G. G., Fillmore, D.,
705 Granier, C., Guenther, A., Kinnison, D., Laepple, T., Orlando, J., Tie, X., Tyndall, G.,
706 Wiedinmyer, C., Baughcum, S. L., and Kloster, S.: Description and evaluation of the Model
707 for Ozone and Related chemical Tracers, version 4 (MOZART-4), *Geoscientific Model*
708 *Development*, 3, 43-67, doi:10.5194/gmd-3-43-2010, 2010.
- 709 Fast, J. D., Gustafson, W. I., Easter, R. C., Zaveri, R. A., Barnard, J. C., Chapman, E. G.,
710 Grell, G. A., and Peckham, S. E.: Evolution of ozone, particulates, and aerosol direct
711 radiative forcing in the vicinity of Houston using a fully coupled meteorology-chemistry-

- 712 aerosol model, *Journal of Geophysical Research: Atmospheres*, 111, D21305,
713 10.1029/2005JD006721, 2006.
- 714 Fioletov, V. E., McLinden, C. A., Krotkov, N., Moran, M. D., and Yang, K.: Estimation of
715 SO₂ emissions using OMI retrievals, *Geophysical Research Letters*, 38, L21811,
716 10.1029/2011GL049402, 2011.
- 717 Flores, J. M., Bar-Or, R. Z., Bluvshstein, N., Abo-Riziq, A., Kostinski, A., Borrmann, S.,
718 Koren, I., Koren, I., and Rudich, Y.: Absorbing aerosols at high relative humidity: linking
719 hygroscopic growth to optical properties, *Atmospheric Chemistry and Physics*, 12, 5511-
720 5521, 10.5194/acp-12-5511-2012, 2012.
- 721 Grell, G. A., and Dévényi, D.: A generalized approach to parameterizing convection
722 combining ensemble and data assimilation techniques, *Geophysical Research Letters*, 29, 38-
723 31-38-34, 10.1029/2002GL015311, 2002.
- 724 Grell, G. A., Peckham, S. E., Schmitz, R., McKeen, S. A., Frost, G., Skamarock, W. C., and
725 Eder, B.: Fully coupled "online" chemistry within the WRF model, *Atmospheric
726 Environment*, 39, 6957-6975, 10.1016/j.atmosenv.2005.04.027, 2005.
- 727 Grell, G. A., and Freitas, S. R.: A scale and aerosol aware stochastic convective
728 parameterization for weather and air quality modeling, *Atmospheric Chemistry and Physics*,
729 14, 5233-5250, 10.5194/acp-14-5233-2014, 2014.
- 730 Guenther, A., Zimmerman, P., and Wildermuth, M.: Natural volatile organic compound
731 emission rate estimates for U.S. woodland landscapes, *Atmospheric Environment*, 28, 1197-
732 1210, 10.1016/1352-2310(94)90297-6, 1994.
- 733 Guenther, A. B., Zimmerman, P. R., Harley, P. C., Monson, R. K., and Fall, R.: Isoprene and
734 monoterpene emission rate variability: model evaluations and sensitivity analyses, *Journal of
735 Geophysical Research-Atmospheres*, 98, 12609-12617, 10.1029/93jd00527, 1993.
- 736 Gustafson, W. I., Qian, Y., and Fast, J. D.: Downscaling aerosols and the impact of neglected
737 subgrid processes on direct aerosol radiative forcing for a representative global climate model
738 grid spacing, *Journal of Geophysical Research: Atmospheres*, 116, D13303,
739 10.1029/2010JD015480, 2011.
- 740 Hand, J. L., Schichtel, B. A., Pitchford, M., Malm, W. C., and Frank, N. H.: Seasonal
741 composition of remote and urban fine particulate matter in the United States, *Journal of
742 Geophysical Research-Atmospheres*, 117, 10.1029/2011jd017122, 2012.
- 743 Hong, S.-Y., Dudhia, J., and Chen, S.-H.: A Revised Approach to Ice Microphysical
744 Processes for the Bulk Parameterization of Clouds and Precipitation, *Monthly Weather
745 Review*, 132, 103-120, doi:10.1175/1520-0493(2004)132<0103:ARATIM>2.0.CO;2, 2004.
- 746 Hyer, E. J., Reid, J. S., and Zhang, J.: An over-land aerosol optical depth data set for data
747 assimilation by filtering, correction, and aggregation of MODIS Collection 5 optical depth
748 retrievals, *Atmospheric Measurement Techniques*, 4, 379-408, 10.5194/amt-4-379-2011,
749 2011.

- 750 Janjić, Z. I.: The Step-Mountain Eta Coordinate Model: Further Developments of the
751 Convection, Viscous Sublayer, and Turbulence Closure Schemes, *Monthly Weather Review*,
752 122, 927-945, doi:10.1175/1520-0493(1994)122<0927:TSMECM>2.0.CO;2, 1994.
- 753 Janjić, Z. I.: Nonsingular implementation of the Mellor–Yamada level 2.5 scheme in the
754 NCEP Meso model, NCEP office note, 437, 61, 2002.
- 755 Jankov, I., A. Gallus, J. W., Segal, M., Shaw, B., and E. Koch, S.: The Impact of Different
756 WRF Model Physical Parameterizations and Their Interactions on Warm Season MCS
757 Rainfall, *Weather and Forecasting*, 20, 1048-1060, doi:10.1175/WAF888.1, 2005.
- 758 Jordan, N. S., Hoff, R. M., and Bacmeister, J. T.: Validation of Goddard Earth Observing
759 System-version 5 MERRA planetary boundary layer heights using CALIPSO, *Journal of*
760 *Geophysical Research-Atmospheres*, 115, 10.1029/2009jd013777, 2010.
- 761 Krotkov, N. A., McClure, B., Dickerson, R. R., Carn, S. A., Li, C., Bhartia, P. K., Yang, K.,
762 Krueger, A. J., Li, Z., Levelt, P. F., Chen, H., Wang, P., and Lu, D.: Validation of SO₂
763 retrievals from the Ozone Monitoring Instrument over NE China, *Journal of Geophysical*
764 *Research: Atmospheres*, 113, D16S40, 10.1029/2007JD008818, 2008.
- 765 Leibensperger, E., Mickley, L. J., Jacob, D. J., Chen, W.-T., Seinfeld, J., Nenes, A., Adams,
766 P., Streets, D., Kumar, N., and Rind, D.: Climatic effects of 1950–2050 changes in US
767 anthropogenic aerosols–Part 1: Aerosol trends and radiative forcing, *Atmospheric Chemistry*
768 *and Physics*, 12, 3333-3348, doi:10.5194/acp-12-3333-2012, 2012.
- 769 Levy, R. C., Mattoo, S., Munchak, L. A., Remer, L. A., Sayer, A. M., Patadia, F., and Hsu, N.
770 C.: The Collection 6 MODIS aerosol products over land and ocean, *Atmospheric*
771 *Measurement Techniques*, 6, 2989-3034, 10.5194/amt-6-2989-2013, 2013.
- 772 Li, L. F., Li, W. H., and Jin, J. M.: Improvements in WRF simulation skills of southeastern
773 United States summer rainfall: physical parameterization and horizontal resolution, *Climate*
774 *Dynamics*, 43, 2077-2091, 10.1007/s00382-013-2031-2, 2014.
- 775 Long, M., Yantosca, R., Nielsen, J., Keller, C., da Silva, A., Sulprizio, M., Pawson, S., and
776 Jacob, D.: Development of a grid-independent GEOS-Chem chemical transport model (v9-
777 02) as an atmospheric chemistry module for Earth system models, *Geoscientific Model*
778 *Development*, 8, 595-602, doi:10.5194/gmd-8-595-2015, 2015.
- 779 Lowrey, M. R. K., and Yang, Z. L.: Assessing the Capability of a Regional-Scale Weather
780 Model to Simulate Extreme Precipitation Patterns and Flooding in Central Texas, *Weather*
781 *and Forecasting*, 23, 1102-1126, 10.1175/2008waf2006082.1, 2008.
- 782 Mann, G. W., Carslaw, K. S., Ridley, D. A., Spracklen, D. V., Pringle, K. J., Merikanto, J.,
783 Korhonen, H., Schwarz, J. P., Lee, L. A., Manktelow, P. T., Woodhouse, M. T., Schmidt, A.,
784 Breider, T. J., Emmerson, K. M., Reddington, C. L., Chipperfield, M. P., and Pickering, S. J.:
785 Intercomparison of modal and sectional aerosol microphysics representations within the same
786 3-D global chemical transport model, *Atmospheric Chemistry and Physics*, 12, 4449-4476,
787 10.5194/acp-12-4449-2012, 2012.
- 788 Martin, S. T., Hung, H. M., Park, R. J., Jacob, D. J., Spurr, R. J. D., Chance, K. V., and Chin,
789 M.: Effects of the physical state of tropospheric ammonium-sulfate-nitrate particles on global

- 790 aerosol direct radiative forcing, *Atmospheric Chemistry and Physics*, 4, 183-214,
791 doi:10.5194/acp-4-183-2004, 2004.
- 792 McComiskey, A., Schwartz, S. E., Schmid, B., Guan, H., Lewis, E. R., Ricchiazzi, P., and
793 Ogren, J. A.: Direct aerosol forcing: Calculation from observables and sensitivities to inputs,
794 *Journal of Geophysical Research: Atmospheres*, 113, D09202, 10.1029/2007JD009170, 2008.
- 795 McLinden, C. A., Fioletov, V., Boersma, K. F., Kharol, S. K., Krotkov, N., Lamsal, L.,
796 Makar, P. A., Martin, R. V., Veefkind, J. P., and Yang, K.: Improved satellite retrievals of
797 NO₂ and SO₂ over the Canadian oil sands and comparisons with surface measurements,
798 *Atmospheric Chemistry and Physics*, 14, 3637-3656, 10.5194/acp-14-3637-2014, 2014.
- 799 Mearns, L. O., Arritt, R., Biner, S., Bukovsky, M., Stain, S., and NARCCAP team The North
800 American Regional Climate Change Assessment Program: Overview of Phase I Results,
801 *Bulletin of the American Meteorological Society*, 93, 1337-1362, 2012.
- 802 Meehl, G. A., Moss, R., Taylor, K. A., Eyring, V., Stouffer, R. J., Sandrine, B., and Stevens,
803 B.: Climate model intercomparisons: preparing for the next phase, *Eos, Transaction,*
804 *American Geophysical Union*, 95, 77-84, doi:10.1002/2014EO09, 2014.
- 805 Misenis, C., and Zhang, Y.: An examination of sensitivity of WRF/Chem predictions to
806 physical parameterizations, horizontal grid spacing, and nesting options, *Atmospheric*
807 *Research*, 97, 315-334, 10.1016/j.atmosres.2010.04.005, 2010.
- 808 Mlawer, E. J., Taubman, S. J., Brown, P. D., Iacono, M. J., and Clough, S. A.: Radiative
809 transfer for inhomogeneous atmospheres: RRTM, a validated correlated-k model for the
810 longwave, *Journal of Geophysical Research: Atmospheres*, 102, 16663-16682,
811 10.1029/97JD00237, 1997.
- 812 Molod, A., Takacs, L., Suarez, M., and Bacmeister, J.: Development of the GEOS-5
813 atmospheric general circulation model: evolution from MERRA to MERRA2, *Geoscientific*
814 *Model Development*, 8, 1339-1356, 10.5194/gmd-8-1339-2015, 2015.
- 815 Murphy, A. H., and Epstein, E. S.: Skill scores and correlation-coefficients in model
816 verification, *Monthly Weather Review*, 117, 572-581, 10.1175/1520-
817 0493(1989)117<0572:ssacci>2.0.co;2, 1989.
- 818 Myhre, G., Samset, B. H., Schulz, M., Balkanski, Y., Bauer, S., Bernsten, T. K., Bian, H.,
819 Bellouin, N., Chin, M., Diehl, T., Easter, R. C., Feichter, J., Ghan, S. J., Hauglustaine, D.,
820 Iversen, T., Kinne, S., Kirkevåg, A., Lamarque, J. F., Lin, G., Liu, X., Lund, M. T., Luo, G.,
821 Ma, X., van Noije, T., Penner, J. E., Rasch, P. J., Ruiz, A., Seland, O., Skeie, R. B., Stier, P.,
822 Takemura, T., Tsigaridis, K., Wang, P., Wang, Z., Xu, L., Yu, H., Yu, F., Yoon, J. H., Zhang,
823 K., Zhang, H., and Zhou, C.: Radiative forcing of the direct aerosol effect from AeroCom
824 Phase II simulations, *Atmospheric Chemistry and Physics*, 13, 1853-1877, 10.5194/acp-13-
825 1853-2013, 2013a.
- 826 Myhre, G., Shindell, D., Bréon, F.-M., Collins, W., Fuglestedt, J., Huang, J., Koch, D.,
827 Lamarque, J.-F., Lee, D., Mendoza, B., Nakajima, T., Robock, A., Stephens, G., Takemura,
828 T., and Zhang, H.: Anthropogenic and Natural Radiative Forcing, in: *Climate Change 2013:*
829 *The Physical Science Basis. Contribution of Working Group I to the Fifth Assessment Report*
830 *of the Intergovernmental Panel on Climate Change*, edited by: Stocker, T. F., Qin, D.,

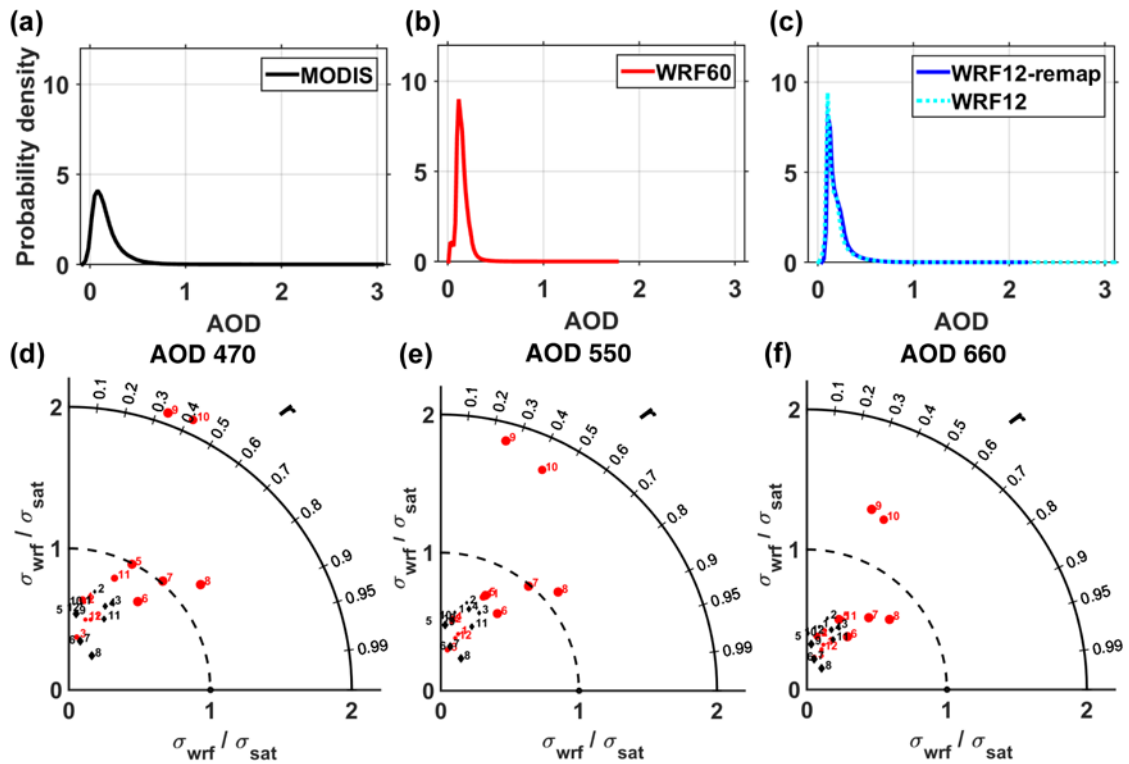
- 831 Plattner, G.-K., Tignor, M., Allen, S. K., Boschung, J., Nauels, A., Xia, Y., Bex, V., and
832 Midgley, P. M., Cambridge University Press, Cambridge, United Kingdom and New York,
833 NY, USA, 659–740, 2013b.
- 834 Nasrollahi, N., AghaKouchak, A., Li, J. L., Gao, X. G., Hsu, K. L., and Sorooshian, S.:
835 Assessing the Impacts of Different WRF Precipitation Physics in Hurricane Simulations,
836 *Weather and Forecasting*, 27, 1003-1016, 10.1175/waf-d-10-05000.1, 2012.
- 837 Qian, Y., Gustafson Jr, W. I., and Fast, J. D.: An investigation of the sub-grid variability of
838 trace gases and aerosols for global climate modeling, *Atmospheric Chemistry and Physics*,
839 10, 6917-6946, 10.5194/acp-10-6917-2010, 2010.
- 840 Rissman, J., Arunachalam, S., Woody, M., West, J. J., BenDor, T., and Binkowski, F. S.: A
841 plume-in-grid approach to characterize air quality impacts of aircraft emissions at the
842 Hartsfield–Jackson Atlanta International Airport, *Atmospheric Chemistry and Physics*, 13,
843 9285-9302, 10.5194/acp-13-9285-2013, 2013.
- 844 Rockel, B., Castro, C. L., Pielke, R. A., von Storch, H., and Leoncini, G.: Dynamical
845 downscaling: Assessment of model system dependent retained and added variability for two
846 different regional climate models, *Journal of Geophysical Research: Atmospheres*, 113,
847 D21107, 10.1029/2007JD009461, 2008.
- 848 Santarpia, J. L., Gasparini, R., Li, R. J., and Collins, D. R.: Diurnal variations in the
849 hygroscopic growth cycles of ambient aerosol populations, *Journal of Geophysical Research-
850 Atmospheres*, 110, 10.1029/2004jd005279, 2005.
- 851 Schell, B., Ackermann, I. J., Hass, H., Binkowski, F. S., and Ebel, A.: Modeling the
852 formation of secondary organic aerosol within a comprehensive air quality model system,
853 *Journal of Geophysical Research-Atmospheres*, 106, 28275-28293, 10.1029/2001jd000384,
854 2001.
- 855 Schuster, G. L., Dubovik, O., and Holben, B. N.: Angstrom exponent and bimodal aerosol
856 size distributions, *Journal of Geophysical Research-Atmospheres*, 111, D07207,
857 doi:10.1029/2005JD006328., 2006.
- 858 Seinfeld, J. H., and Pandis, S. N.: *Atmospheric chemistry and physics: from air pollution to
859 climate change*, John Wiley & Sons, 1152 pp., 2016.
- 860 Simes, R. J.: An improved Bonferroni procedure for multiple tests of significance,
861 *Biometrika*, 73, 751-754, 10.2307/2336545, 1986.
- 862 Simpson, D., Guenther, A., Hewitt, C. N., and Steinbrecher, R.: Biogenic emissions in
863 Europe. 1. estimates and uncertainties, *Journal of Geophysical Research-Atmospheres*, 100,
864 22875-22890, 10.1029/95jd02368, 1995.
- 865 Stocker, T. F. a. Q., D. and Plattner, G.-K. and Alexander, L.V. and Allen, S.K. and Bindoff,
866 N.L. and Bréon, F.-M. and Church, J.A. and Cubasch, U. and Emori, S. and Forster, P. and
867 Friedlingstein, P. and Gillett, N. and Gregory, J.M. and Hartmann, D.L. and Jansen, E. and
868 Kirtman, B. and Knutti, R. and Krishna Kumar, K. and Lemke, P. and Marotzke, J. and
869 Masson-Delmotte, V. and Meehl, G.A. and Mokhov, I.I. and Piao, S. and Ramaswamy, V.
870 and Randall, D. and Rhein, M. and Rojas, M. and Sabine, C. and Shindell, D. and Talley,

- 871 L.D. and Vaughan, D.G. and Xie, S.-P.: Summary for Policymakers, in: Climate Change
 872 2013: The Physical Science Basis. Contribution of Working Group I to the Fifth Assessment
 873 Report of the Intergovernmental Panel on Climate Change, Cambridge University Press,
 874 Cambridge, United Kingdom and New York, NY, USA, 33–115, 2013.
- 875 Stockwell, W. R., Middleton, P., Chang, J. S., and Tang, X.: The second generation regional
 876 acid deposition model chemical mechanism for regional air quality modeling, *Journal of*
 877 *Geophysical Research: Atmospheres*, 95, 16343-16367, 10.1029/JD095iD10p16343, 1990.
- 878 Sun, Y., Yi, L., Zhong, Z., and Ha, Y.: Performance of a New Convective Parameterization
 879 Scheme on Model Convergence in Simulations of a Tropical Cyclone at Grey-Zone
 880 Resolutions, *Journal of the Atmospheric Sciences*, 71, 2078-2088, doi:10.1175/JAS-D-13-
 881 0285.1, 2014.
- 882 Taylor, K. E.: Summarizing multiple aspects of model performance in a single diagram,
 883 *Journal of Geophysical Research-Atmospheres*, 106, 7183-7192, 10.1029/2000jd900719,
 884 2001.
- 885 Textor, C., Schulz, M., Guibert, S., Kinne, S., Balkanski, Y., Bauer, S., Berntsen, T., Berglen,
 886 T., Boucher, O., Chin, M., Dentener, F., Diehl, T., Easter, R., Feichter, H., Fillmore, D.,
 887 Ghan, S., Ginoux, P., Gong, S., Kristjansson, J. E., Krol, M., Lauer, A., Lamarque, J. F., Liu,
 888 X., Montanaro, V., Myhre, G., Penner, J., Pitari, G., Reddy, S., Seland, O., Stier, P.,
 889 Takemura, T., and Tie, X.: Analysis and quantification of the diversities of aerosol life cycles
 890 within AeroCom, *Atmospheric Chemistry and Physics*, 6, 1777-1813, 2006.
- 891 Tilmes, S., Lamarque, J.-F., Emmons, L., Kinnison, D., Ma, P.-L., Liu, X., Ghan, S.,
 892 Bardeen, C., Arnold, S., and Deeter, M.: Description and evaluation of tropospheric
 893 chemistry and aerosols in the Community Earth System Model (CESM1. 2), *Geoscientific*
 894 *Model Development*, 8, 1395-1426, doi:10.5194/gmd-8-1395-2015, 2015.
- 895 Tomasi, C., Caroli, E., and Vitale, V.: Study of the Relationship between Ångström's
 896 Wavelength Exponent and Junge Particle Size Distribution Exponent, *Journal of Climate and*
 897 *Applied Meteorology*, 22, 1707-1716, 10.1175/1520-
 898 0450(1983)022<1707:SOTRBW>2.0.CO;2, 1983.
- 899 US-EPA: 2005 National Emissions Inventory (NEI), US Environmental Protection Agency
 900 in, available at: ftp://aftp.fsl.noaa.gov/divisions/taq/emissions_data_2005/, 2009.
- 901 Vinken, G. C. M., Boersma, K. F., van Donkelaar, A., and Zhang, L.: Constraints on ship
 902 NO_x emissions in Europe using GEOS-Chem and OMI satellite NO₂ observations,
 903 *Atmospheric Chemistry and Physics*, 14, 1353-1369, 10.5194/acp-14-1353-2014, 2014.
- 904 von Engel, A., and Teixeira, J.: A Planetary Boundary Layer Height Climatology Derived
 905 from ECMWF Reanalysis Data, *Journal of Climate*, 26, 6575–6590, doi: 10.1175/JCLI-D-12-
 906 00385.1, 2013.
- 907 Weigum, N., Schutgens, N., and Stier, P.: Effect of aerosol sub-grid variability on aerosol
 908 optical depth and cloud condensation nuclei: Implications for global aerosol modelling,
 909 *Atmos. Chem. Phys. Discuss.*, 2016, 1-36, 10.5194/acp-2016-360, 2016.

- 910 Whitburn, S., Van Damme, M., Clarisse, L., Bauduin, S., Heald, C., Hadji-Lazaro, J.,
911 Hurtmans, D., Zondlo, M. A., Clerbaux, C., and Coheur, P.-F.: A flexible and robust neural
912 network IASI-NH₃ retrieval algorithm, *Journal of Geophysical Research-Atmospheres*, In
913 Press, 10.1002/2016JD024828, 2016.
- 914 Wild, O., Zhu, X., and Prather, M. J.: Fast-J: Accurate Simulation of In- and Below-Cloud
915 Photolysis in Tropospheric Chemical Models, *Journal of Atmospheric Chemistry*, 37, 245-
916 282, 10.1023/a:1006415919030, 2000.
- 917 Zhang, X., Chen, Z. M., Wang, H. L., He, S. Z., and Huang, D. M.: An important pathway for
918 ozonolysis of alpha-pinene and beta-pinene in aqueous phase and its atmospheric
919 implications, *Atmospheric Environment*, 43, 4465-4471, 10.1016/j.atmosenv.2009.06.028,
920 2009.
- 921 Zhang, Y., He, J., Zhu, S., and Gantt, B.: Sensitivity of simulated chemical concentrations
922 and aerosol-meteorology interactions to aerosol treatments and biogenic organic emissions in
923 WRF/Chem, *Journal of Geophysical Research: Atmospheres*, 121, 6014-6048,
924 10.1002/2016JD024882, 2016.
- 925 Zieger, P., Fierz-Schmidhauser, R., Weingartner, E., and Baltensperger, U.: Effects of
926 relative humidity on aerosol light scattering: results from different European sites,
927 *Atmospheric Chemistry and Physics*, 13, 10609-10631, 10.5194/acp-13-10609-2013, 2013.
- 928
- 929

930 **Figures**

931



932

933 **Figure 1. Probability density function of once daily AOD at a wavelength (λ) of 550 nm**

934 **for (a) MODIS, (b) WRF60 and (c) WRF12 and WRF12-remap during the year 2008.**

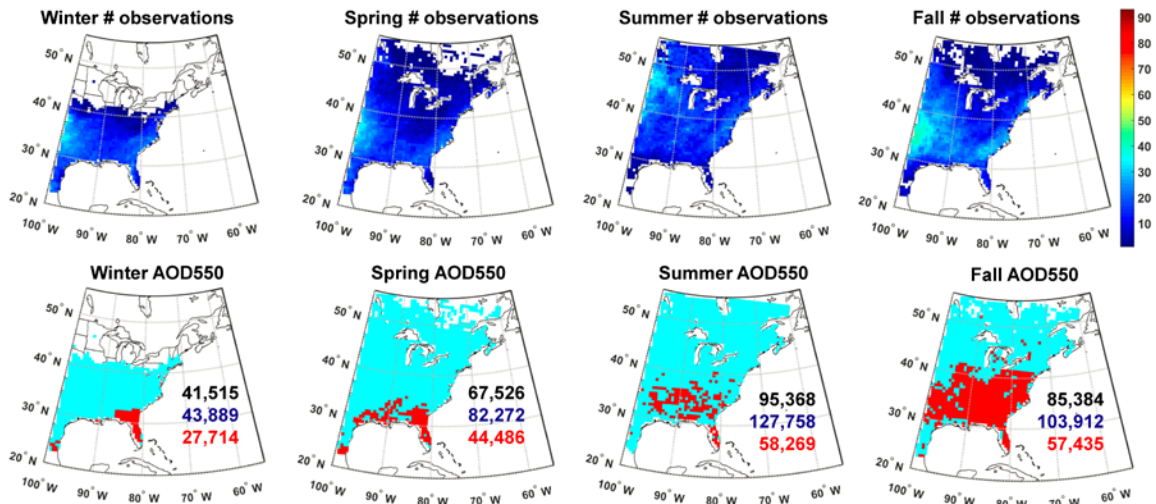
935 **(d-f) Taylor diagrams of mean monthly AOD at wavelengths (λ) of (d) 470, (e) 550 and**

936 **660 nm as simulated by WRF-Chem at different resolutions (black**

937 **diamonds=WRF60 and red dots=WRF12-remap) relative to MODIS observations. The**

938 **numbers by each symbol denote the calendar month (e.g. 1=January).**

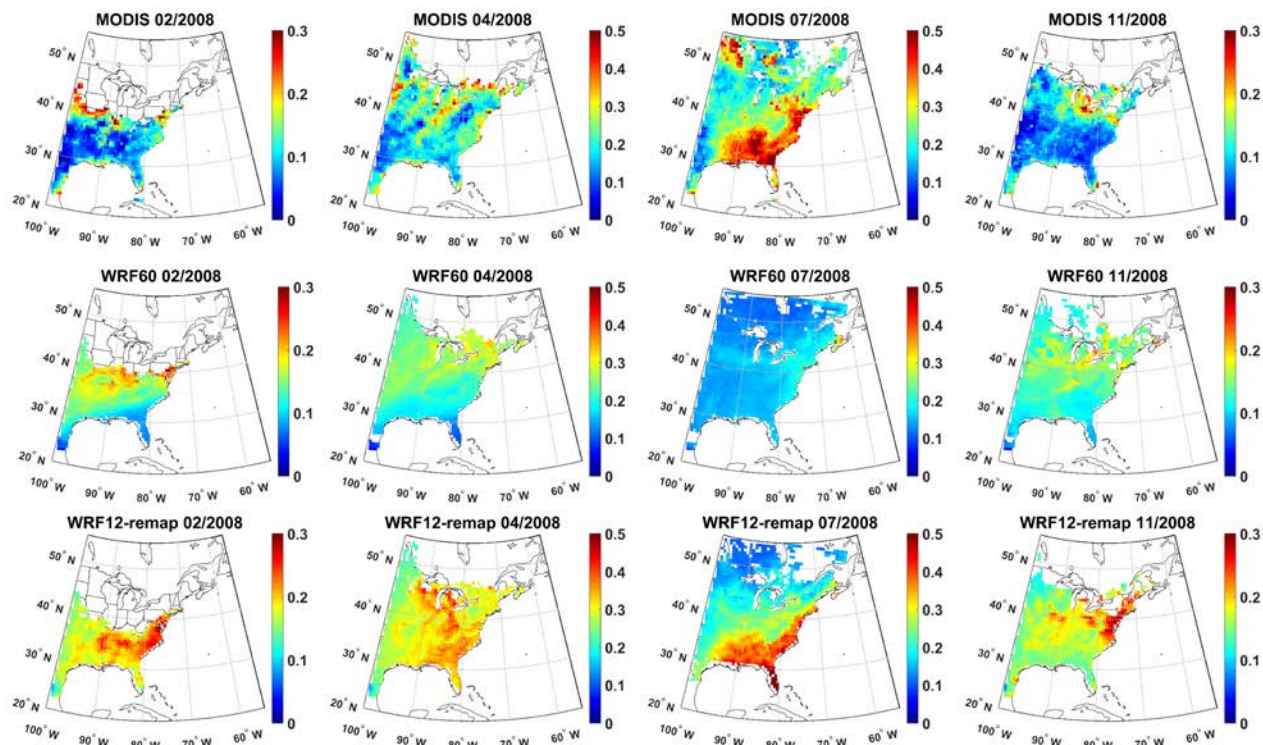
939



940

941 **Figure 2. First line: Number of paired AOD observations at a wavelength (λ) of 550 nm**
 942 **(i.e. simultaneous values as output from WRF-Chem and observed by MODIS) used to**
 943 **perform a t-test designed to evaluate whether the difference computed for each grid cell**
 944 **as WRF60-MODIS differs from that computed as WRF12-remap-MODIS on a seasonal**
 945 **basis (columns show Winter (DJF), Spring (MAM), Summer (JJA) and Fall (SON)).**
 946 **Second line: Results of the t-test. Pixels that have p-values that are significantly**
 947 **different at $\alpha=0.10$ are indicated in red and have been corrected for multiple testing**
 948 **using a False Discovery Rate approach. The number of observations of cloud-free**
 949 **conditions summed across all days in each season and all grid cells is also reported**
 950 **(black=MODIS, blue=WRF60, red=WRF12-remap).**

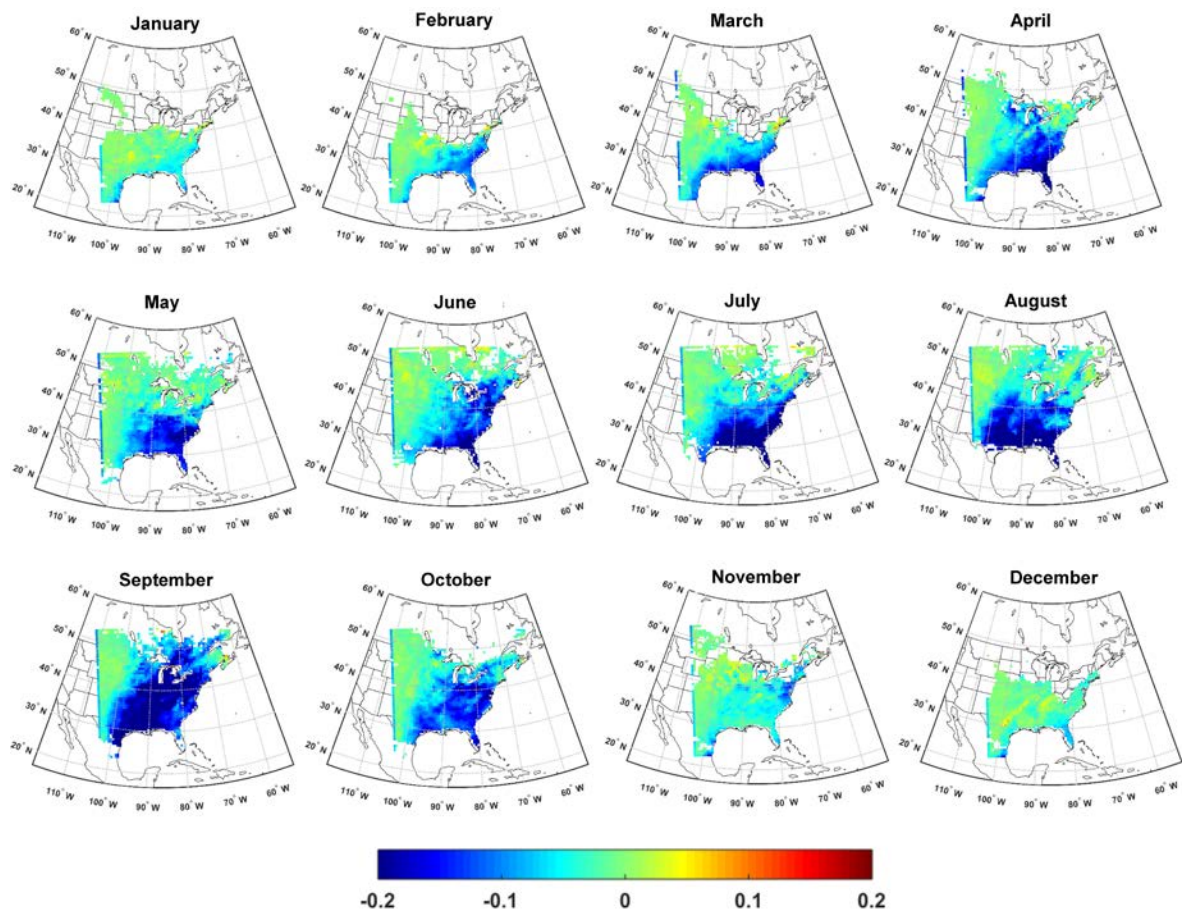
951



952

953 **Figure 3. Monthly mean AOD at a wavelength (λ) of 550 nm from MODIS (first line)**
 954 **and WRF-Chem at different resolutions (WRF60 and WRF12-remap, second and third**
 955 **line) during a representative month in each climatological season (columns). Note that a**
 956 **different color scale is applied for different months. For a monthly mean value for a**
 957 **grid cell to be shown, there must be at least 5-simultaneous daily values (for the time of**
 958 **the satellite overpass) available.**

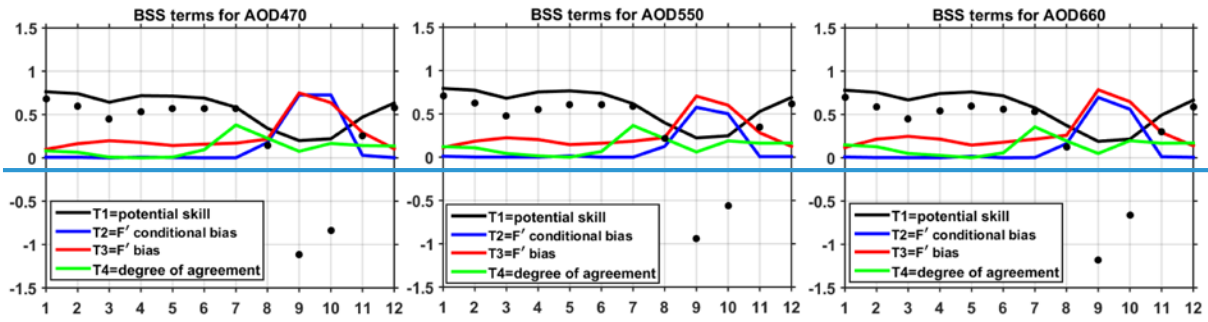
959



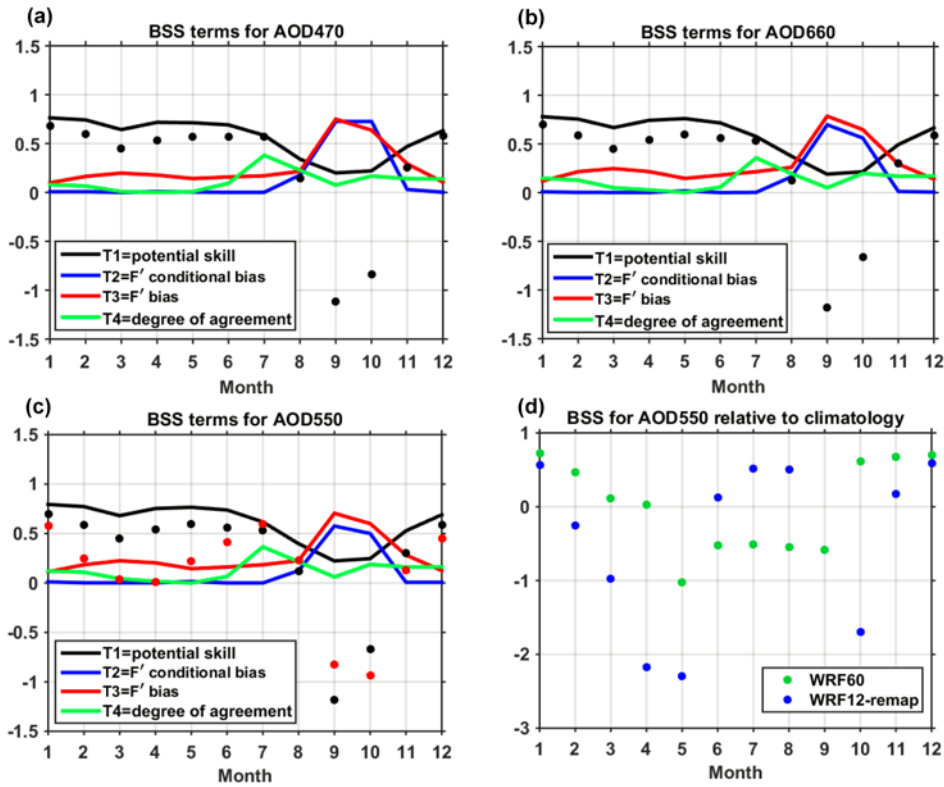
960

961 **Figure 4. Difference in monthly mean AOD at a wavelength (λ) of 550 nm between**
 962 **WRF-Chem simulations conducted at 60 km resolution (WRF60) and output from**
 963 **WRF-Chem simulations conducted with a resolution of 12 km but remapped to 60 km**
 964 **(WRF12-remap). Differences are computed as WRF60 minus WRF12-remap. Similar**
 965 **spatial patterns and magnitudes of differences are found for λ of 470 and 660 nm. The**
 966 **calendar months of 2008 are shown in the titles of each panel.**

967



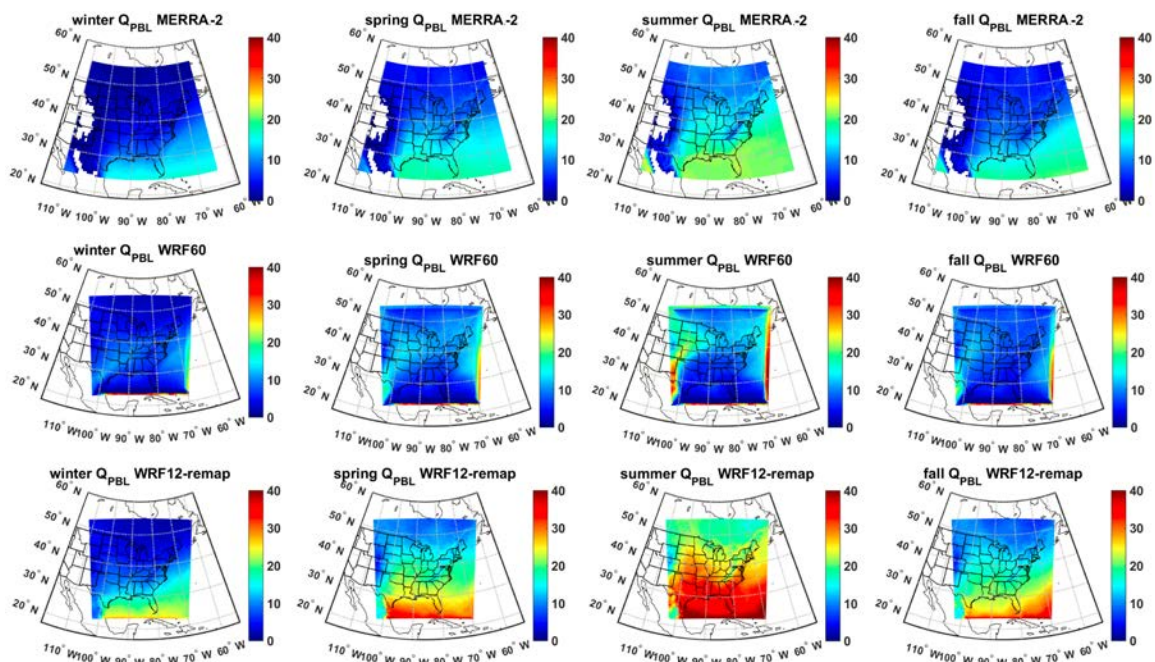
968



969

970 **Figure 5. (a-c) Brier Skill Scores (BSS, black black-dots)** for monthly mean AOD by
 971 **calendar month (1=January)** for AOD at 470, 550 and 660 nm. In this analysis of model
 972 **skill WRF12 output is mapped to the WRF60 grid (WRF12-remap)** and BSS are
 973 **computed using MODIS as the target, WRF60 (driven by NAM12 meteorological**
 974 **boundary conditions)** as the reference forecast and WRF12-remap as the forecast. Also
 975 **shown by the color lines are the contributions of different terms to BSS. In panel c the**
 976 **red dots indicate BSS when the reference forecast is WRF60 driven by GFS**
 977 **meteorological boundary conditions. (d) BSS of monthly mean AOD from WRF60**
 978 **(green dots) and WRF12-remap (blue dots) relative to MODIS monthly mean**
 979 **climatology during 2000-2014 (reference forecast). Monthly mean AOD from MODIS**
 980 **are used as the target. BSS for WRF12-remap in September is -6.1.**

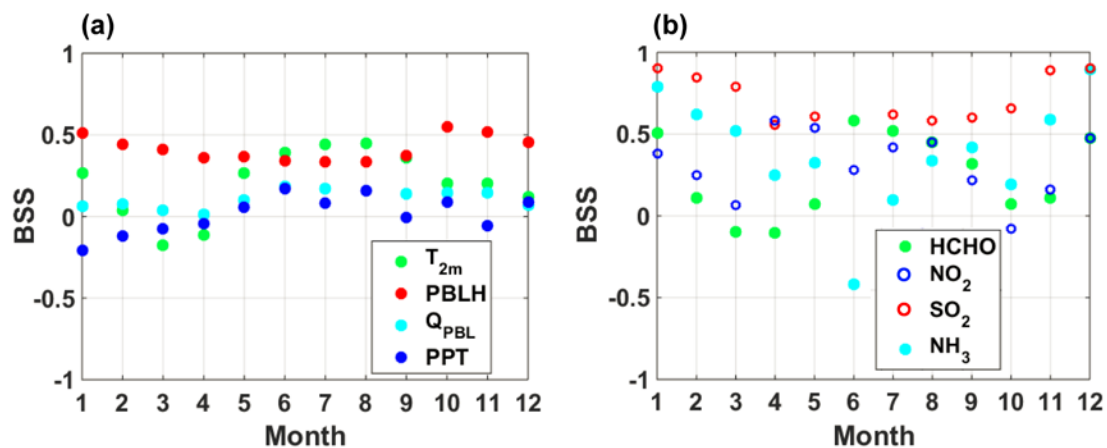
981
|
982



983

984 **Figure 6.** Seasonal mean specific humidity [kg m^{-2}] integrated from the surface to 825
 985 hPa (Q_{PBL}) from MERRA-2 (first row) assuming an average air density in the *PBL* of
 986 1.1 kg m^{-3} , WRF60 (second row), and WRF12-remap (third row). The data are 3-hourly
 987 and show only cloud-free hours in all three data sets.

988



989

990 **Figure 7. Brier Skill Scores (BSS) for key (a) meteorological and (b) chemical variables.**

991 **BSS are computed using hourly data of T at 2m (T_{2m}) and PBLH, 3-hourly estimates of**
 992 **specific humidity in the boundary layer (Q_{PBL}), and z-scores of monthly total**
 993 **precipitation (PPT), and of monthly mean columnar gas phase concentrations.**

994

995

997 **Table 1. Physical and chemical schemes adopted in the WRF-Chem simulations**
 998 **presented herein.**

Simulation settings	Values
Domain size	300 × 300 (60 × 60) grid points
Horizontal resolution	12 km (60 km)
Vertical resolution	32 levels up to 50 hPa
Timestep for physics	72 s (300 s)
Timestep for chemistry	5 s
Physics option	Adopted scheme
Microphysics	WRF Single-Moment 5-class (Hong et al., 2004)
Longwave Radiation	Rapid Radiative Transfer Model (RRTM) (Mlawer et al., 1997)
Shortwave Radiation	Goddard (Fast et al., 2006)
Surface layer	Monin Obhukov similarity (Janjić, 2002; Janjić, 1994)
Land Surface	Noah Land Surface Model (Chen and Dudhia, 2001)
Planetary boundary layer	Mellor-Yamada-Janjich (Janjić, 1994)
Cumulus parameterizations	Grell 3D (Grell and Dévényi, 2002)
Chemistry option	Adopted scheme
Photolysis	Fast J (Wild et al., 2000)
Gas-phase chemistry	RADM2 (Stockwell et al., 1990)
Aerosols	MADE/SORGAM (Ackermann et al., 1998; Schell et al., 2001)
Anthropogenic emissions	NEI (2005) (US-EPA, 2009)
Biogenic emissions	Guenther, from USGS land use classification (Guenther et al., 1994; Guenther et al., 1993; Simpson et al., 1995)

1001 **Table 2. Spearman correlation coefficients (ρ) between AOD at wavelengths (λ) of 470,**
1002 **550 and 660 nm from MODIS observations averaged over 12 or 60 km and WRF-Chem**
1003 **simulations conducted at 60 km (WRF60, shown in the table as -60), at 12 km (WRF12,**
1004 **shown in the table as -12), and from WRF-Chem simulations at 12 km but remapped to**
1005 **60 km (WRF12-remap, shown in the table as -remap). Given WRF12-remap is obtained**
1006 **by averaging WRF12 when at least half of the 5×5 12 km resolution cells contain valid**
1007 **data, ρ from WRF60 and WRF12-remap may be computed on slightly different**
1008 **observations and sample size. The bold text denotes correlation coefficients that are**
1009 **significant at $\alpha=0.05$ after a Bonferroni correction is applied (i.e.**
1010 $p \leq \frac{0.05}{9 \times 12} = 4.63 \times 10^{-4}$ **is significant). The yellow shading is a visual guide that shows for**
1011 **each month and λ the model output that has highest ρ with MODIS.**

Month→/ Variable↓	Jan	Feb	Mar	Apr	May	Jun	Jul	Aug	Sep	Oct	Nov	Dec
470-12	0.238	0.150	0.137	0.147	0.377	0.581	0.610	0.723	0.352	0.306	0.259	0.212
470-60	0.156	0.226	0.438	0.412	-0.219	-0.146	0.379	0.601	0.087	-0.051	0.500	-0.059
470-remap	0.295	0.197	0.250	0.182	0.516	0.637	0.675	0.777	0.368	0.441	0.315	0.274
550-12	0.223	0.124	0.142	0.146	0.349	0.541	0.580	0.689	0.275	0.301	0.280	0.215
550-60	0.179	0.244	0.429	0.332	-0.288	-0.188	0.324	0.567	0.073	-0.077	0.491	0.002
550-remap	0.297	0.164	0.261	0.199	0.493	0.605	0.651	0.747	0.286	0.437	0.352	0.309
660-12	0.217	0.136	0.165	0.152	0.324	0.476	0.540	0.644	0.183	0.290	0.292	0.221
660-60	0.191	0.230	0.437	0.402	-0.305	-0.189	0.389	0.616	0.099	-0.137	0.536	0.049
660-remap	0.356	0.211	0.289	0.208	0.480	0.624	0.669	0.772	0.371	0.432	0.393	0.368

1012

1013

1014 **Table 3. Spatial coherence in the identification of extreme AOD values (i.e. areas with**
1015 **AOD>75th percentile over space for each month) between WRF-Chem at different**
1016 **resolutions relative to MODIS. No significant wavelength dependence is found for**
1017 **model skill in identifying extreme AOD so results are only shown for $\lambda = 550$ nm. The**
1018 **different model output is denoted by -60 for simulations at 60 km, -12 for simulations at**
1019 **12 km resolution, and as -remap for simulations at 12 km but with the output**
1020 **remapped to 60 km. The *Accuracy* (Acc) indicates the fraction of grid cells co-identified**
1021 **as extremes and non-extremes between WRF-Chem and MODIS relative to the total**
1022 **number of cells with valid data. The *Hit Rate* (HR) is the probability of correct forecast**
1023 **and is the proportion of cells correctly identified as extremes by both WRF-Chem and**
1024 **MODIS. The yellow shading indicates the model resolution with highest skill in each**
1025 **month for AOD at 550 nm.**

Month→/ Metric↓	Jan	Feb	Mar	Apr	May	Jun	Jul	Aug	Sep	Oct	Nov	Dec
Acc-12	0.673	0.665	0.659	0.638	0.710	0.800	0.855	0.839	0.666	0.679	0.723	0.661
Acc-60	0.707	0.778	0.735	0.730	0.600	0.587	0.658	0.769	0.661	0.637	0.729	0.681
Acc-remap	0.674	0.680	0.694	0.640	0.766	0.824	0.887	0.837	0.667	0.699	0.767	0.641
HR-12	0.346	0.331	0.319	0.275	0.421	0.599	0.711	0.678	0.333	0.358	0.447	0.323
HR-60	0.417	0.558	0.471	0.460	0.200	0.173	0.315	0.538	0.321	0.274	0.458	0.364
HR-remap	0.350	0.361	0.387	0.281	0.532	0.649	0.775	0.674	0.333	0.399	0.535	0.284

1026
1027
1028
1029
1030
1031
1032
1033